Institutionen för Vattenbyggnad
Chalmers Tekniska Högskola

Department of Hydraulics
Chalmers University of Technology

ESTIMATING THE TIME TO FATIGUE FAILURE OF MOORING CABLES

by

Wilhelm Rankka

Report
Series A:20
ISSN 0348-1050

Göteborg 1989

Address: Department of Hydraulics
Chalmers University of Technology
S-412 96 Göteborg, Sweden
Telephone: 031 - 72 10 00

SUMMARY

In this report two methods of calculation of the time to fatigue failure of mooring cables are analysed. The methods are based on the theory of cumulative damage and they are applied to the fatigue of catenary cables of wire rope caused by fluctuating axial load. To calculate the cable load a time domain approach is used which includes a simple model of the viscous damping of the platform heave motion. The cable load time history is analysed with the rain flow counting algorithm.

One of the analysed methods is based on a narrow band approximation of the cable load spectrum and the other method makes use of transfer functions from first order wave to cable load. For some of the studied load cases, the narrow band approximation leads to an underestimation of the fatigue damage. It is concluded that transfer functions from first order wave to cable load calculated for one wave–spectrum can be used for other wave–spectra if the cable configuration, the cable mean–load, and the wave direction are not changed.

The S–N curve and the effective modulus of elasticity of the cable are found to be the two most important factors in a calculation of the fatigue damage for a specific load case.

A sample problem of analysing the mooring cables of a semisubmersible in the North Sea is solved by use of the method based on the narrow band assumption. The time to fatigue failure of the most exposed cable was 440 years.

PREFACE

Research concerning wave/structure interaction has been performed at the Department of Hydraulics, Chalmers University of Technology, since the mid 70s. Wave energy devices, offshore structures and harbour units have been included. Since 1980 the National Swedish Board of Technical Development (STU) has sponsored the activities in the project "Offshore Structures – Wave Forces and Motions".

This thesis is the result of a part of the project concerning the fatigue of offshore mooring cables which was co–sponsored by Safe Offshore. The work has been carried out at the Department of Hydraulics and is submitted in partial fulfillment of the requirements for the degree of Technical Licentiate.

I wish to thank my advisor, Professor Lars Bergdahl, for his guidance and support. I am also grateful to Tore Dalväg at Safe Offshore, Göteborg for constructive discussions; to Henriette Melin who helped me with computer operations; and to Anne–Marie Hellgren and Yvonne Young who typed the manuscript.

Göteborg, Maj 1989

Wilhelm Rankka

CONTENTS

1. INTRODUCTION

Fatigue is a common failure mode in engineering structures subjected to varying loads of significant magnitude. Examples of such structures are machines subject to vibrations, bridges subject to fluctuating live loads, and offshore structures subject to varying loads from waves. This study concerns fatigue in mooring cables for offshore structures.

There are two ways to analyse fatigue. The first is to use test results in the form of an S–N curve for the structural member of interest. (S stands for stress or strain, N stands for number of cycles.) An S–N curve shows how many cycles a material can resist before failure as a function of the load–cycle range. A comparison between the S–N curve and an appropriate description of the load will show whether or not the structural member will fail. The second way is to apply fracture mechanics. Fracture mechanics gives information about the progress of failure and involves measures, or estimates, of the rate of crack propagation. Such an analysis is mainly used to assess the remaining life of a structural member beeing inspected after some time in service.

In the study, the first of the two methods mentioned above is used for the calculation of the expected time to fatigue failure of mooring cables for a floating platform. The S–N curve used to characterise the cable is a curve presented in MTD (1988). The curve is based on tests of six strand IWRC wire ropes (see Section 2.2 for definition) in the diameter range 13 mm to 73 mm.

A time domain approach is used to estimate the load. Platform motions are generated according to a first order potential theory (Faltinsen and Michelsen, 1975) and a FEM model, MODEX, by Lindahl (Lindahl and Sjöberg, 1983) is used to calculate the cable load. The platform heave motions are modified by a simple model of viscous damping and the description of the load in terms of number of cycles of different ranges is obtained with the Rainflow Cycle counting algorithm.

1.1 Other studies on the subject

In 1987 the Marine Technology Directorate in Britain initiated a joint industry study of the endurance of large diameter wire ropes used, or proposed for use, in moorings of offshore structures. In one of the reports from the study results from fatigue tests with fluctuating axial load from different authors are presented (MTD, 1988, Figure 8). The results show a large scatter. It is concluded, however, that the scatter is mainly due to the lack of general and well–defined test specifications. In Figure 2.2.2, the most reliable of the results have been plotted relative to a consequent definition of static breaking load. In this figure the scatter is lower.

Corrosion reduces the fatigue life of wire ropes (Zimmerman and Reemsnyder, 1985; Husain and Cottis, 1986). Wire ropes in a marine environment are susceptible to corrosion, especially if they are frequently moved in and out of the water, such as the upper end of a mooring cable. An efficient means of preventing corrosion is zinc coating (Zimmerman and Reemsnyder, 1985).

In Safe Offshore (1986) it is reported that the major reason for replacement of wire ropes on semi–submersibles is wear. An examination of 8 wire ropes used by Safe Offshore during 4 years is reported in Scanrope (1984). A significant reduction of the core diameter had taken place around the touch down point (i.e. where the rope is regularly lifted off and laid down on the bottom) and in the catenary sections. A significant reduction of breaking strength was also noted for samples taken from these sections. The fairlead section and the section close to the anchor were in better condition.

The accuracy of the FEM model MODEX of the wire rope is discussed in Lindahl and Sjöberg (1983), Lindahl (1985) and Bergdahl and Rask (1987). In Lindahl and Sjöberg (1983) MODEX is compared to a FEM model by Johansson (1976) for a two dimensional cable with a fixed lower end. Good agreement between the results was noted. Results from laboratory tests of a model of a chain suspended in a basin are compared with a corresponding MODEX calculation in Lindahl (1985). The MODEX model was two–dimensional and included bottom friction. The difference between the calculated maximum forces and the corresponding measured forces was within the margin of error, which was judged to be around ±16%. The influence of hydrodynamic coefficients on the computations was low.

Bergdahl and Rask studied a combined chain and wire rope system with a prototype diameter of 135 mm. They used the three–dimensional version of the MODEX model and compared the results with laboratory tests performed at SSPA in Göteborg. The computed maximum tension was between 4% and 12% lower than the measured maximum tension. They also noted that horizontal platform motions will be underestimated if second order motions are not taken into account.

1.2 Scope of the report

A wire rope for moorings usually consists of wires of brittle high–strength steel spun together into strands. Such a structure assures an efficient spreading of the load to all the wires and the negative effect of a crack in one wire is limited. Cracks do, however, easily develop in high–strength steel, and large numbers of them reduce the load carrying capacity of the rope.

In MTD (1988) the loadings which can result in fatigue of a mooring cable are divided into three types:

– tension–tension fatigue, i.e.
fluctuating line tension owing to platform movements;

– bending–tension fatigue, i.e.
small amplitude motion and bending of a rope over a fairlead pulley in phase with fluctuating line tensions;

– free bending–tension fatigue, i.e.
change in unsupported rope curvature in phase with fluctuating line tensions which occur near rope terminations.

It is not clear which of the loading types is most important. The study is focused on the tension–tension fatigue of the catenary part of a mooring rope.

In Chapter 7 two methods of calculation of fatigue damage are examined. A sample problem presented in Chapter 2 is used to illustrate and apply the methods. This problem is to predict the time to fatigue failure for a wire rope used in a mooring system for a semisubmersible platform. The semisubmersible platform is moored at a depth of 250 m at Haltenbanken on the Norwegian Shelf.

To determine the cable load a quasi static approach is used and the platform motions due to the first order wave are obtained by time domain simulations. This approach is described in Chapters 3 and 4. The spectral analysis necessary to perform a calculation of the fatigue damage according to the examined methods is presented in Chapter 5. Chapter 6 is a study of how the fatigue damage and the cable load time history vary with respect to sea–state characteristica, hydrodynamic parameters, and cable mean–loads.

The main assumptions in the report are: the first order theory is sufficient to model the waves and the platform motion; the FEM model of the wire rope gives accurate results; a well defined S–N curve for wire ropes can be obtained; the frequency table of significant wave heights and spectral peak periods (OCEANOR, 1987) is a good representation of the environmental forces.

2 SAMPLE PROBLEM

To illustrate the method of calculation a sample problem is studied. This problem is to estimate the fatigue life of the catenary mooring cables of a floating platform located off the Norwegian coast.

2.1 Sample platform, location, and mooring configuration

The sample platform is a semi–submersible of a design called "Pace–Setter". The platform consists of two parallel pontoons, six circular columns and a deck. The length over all is 94 m and the height from keel to deck is 30 m. The platform can be operated at three different draughts: transit, operational and survival. Transit draught means that the pontoons of the platform are at level with the water surface. Transit draught is used to move the platform to and from areas of operation. In operational draught the platform is ballasted to bring the pontoons well under the water surface, and the movements due to waves are thereby minimized. Survival draught means that the platform is deballasted to a level between transit draught and operational draught. Survival draught is used in extreme weather conditions to minimize the risk of storm waves hitting the deck. Figure 2.1.1 is a side view of the platform.

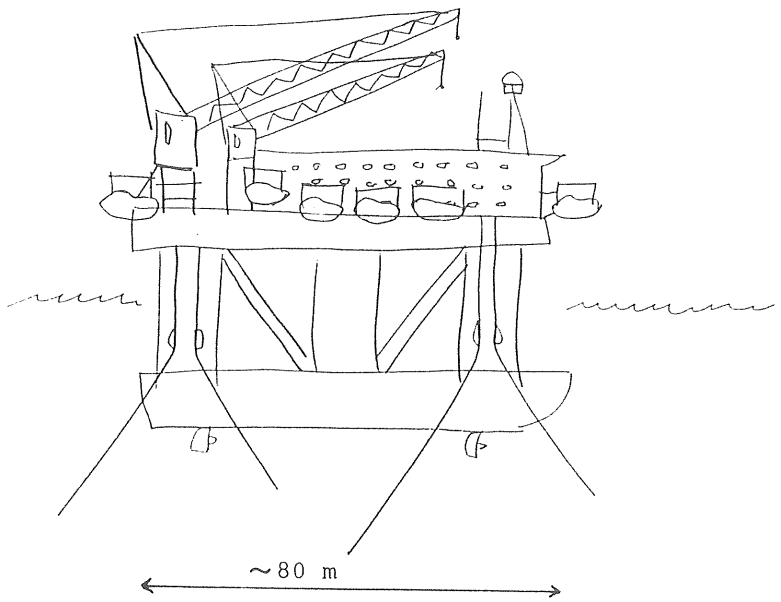

Figure 2.1.1 Sideview of the sample platform.

The platform is moored at Haltenbanken (65^{0}05' N 07^{0}34' E) off the Norwegian coast at a water depth of 250 m. The mooring pattern is shown in Figure 2.1.2 and tabulated below. The platform is moored next to a fixed installation, to which it is connected by a gangway. In calm weather the distance between the platform and the installation is about 30 m. This position is called the operational position. When the swaying of the gangway becomes too great owing to bad weather, the gangway is disconnected, and the platform is hauled to a distance of about 100 m from the installation. This position is called the stand–off position. In extreme weather conditions, the platform is also raised to survival draught.

Some important data for the platform are the following.

Pontoon length:	79.6	m	
Pontoon beam:	15.2	m	
Pontoon height:	6.1	m	
Volume of the immersed part:	20 390	m^3	(operational draught)
	18 010	m^3	(survival draught)
Water plane area:	530	m^2	(operational draught)
	500	m^2	(survival draught)
Area used for the calculation of viscous damping in heave, A:	2100	m^2	
Heave damping coefficent, C_{D3}:	1.0		

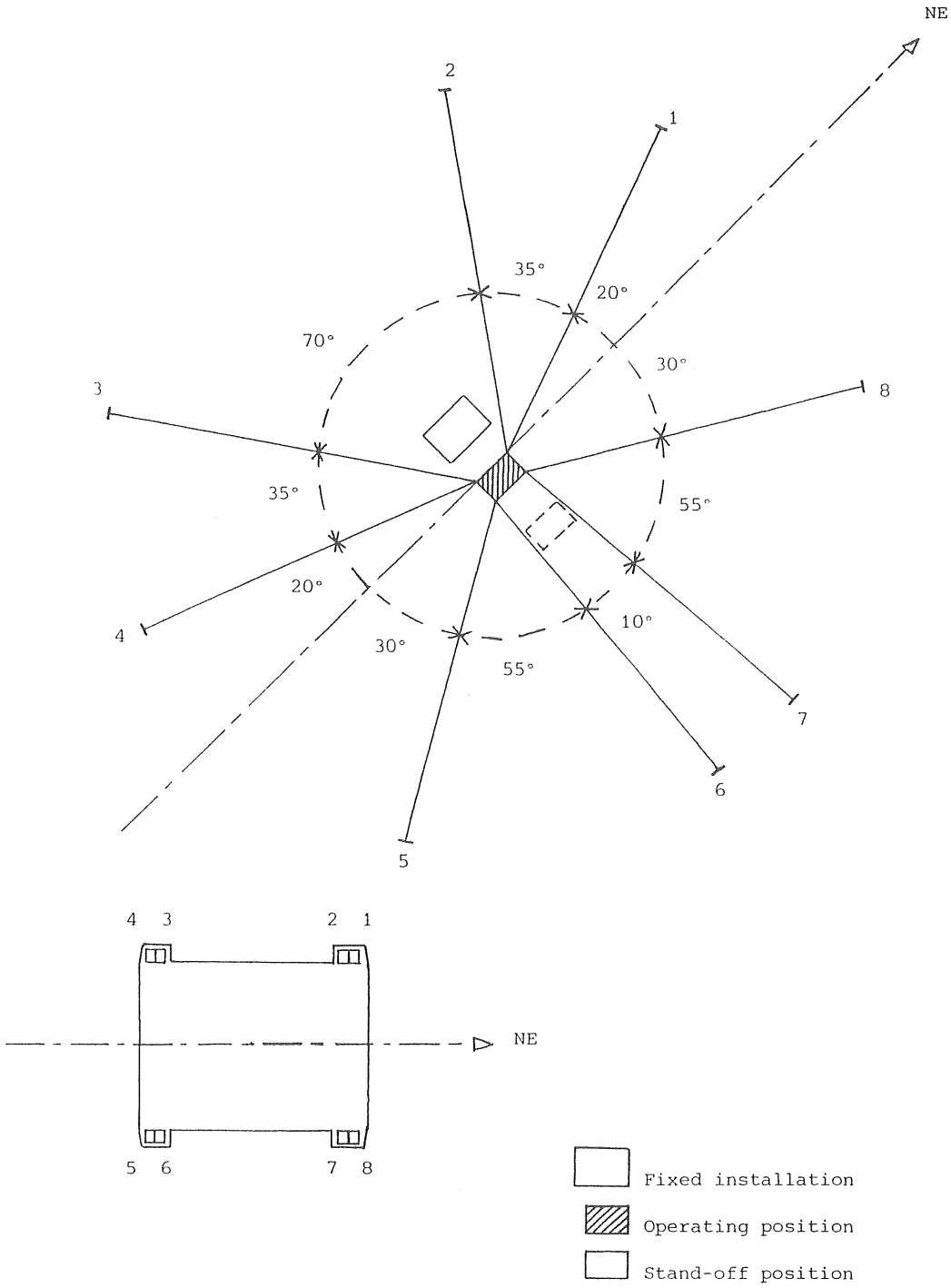

Figure 2.1.2 Mooring pattern and fairlead numbering.

Table 2.1.1 Fairleads in the coordinate system B (see app. 3).

Fairlead no	Horizontal distance from origin (m)	Horizontal direction (deg)	Vertical coord (m) operation	survival
1	40.46	43.80	–4.0	–0.2
2	37.80	47.79	"	"
3	37.80	132.21	"	"
4	40.46	136.20	"	"
5	40.46	223.80	"	"
6	37.80	227.79	"	"
7	37.80	312.21	"	"
8	40.46	316.20	"	"

Table 2.1.2 Operational position in a coordinate system G (see app. 3) which has its origin at the operational position, and its x–axis in the NE direction.

Anchor no	From fairlead no	Horizontal distance (m)	Direction (deg)
1.1	1	1830	20
2.1	2	1790	55
3.1	3	1790	55
4.1	4	1830	160
5.1	5	1900	210
6.1	6	1900	265
7.1	7	1900	275
8.1	8	1900	330

Table 2.1.3 Stand–off position in a coordinate system G (see app. 3) which has its origin at the stand off position, and its x–axis in the E direction.

Anchor no	From fairlead no	Distance (m)	Direction (deg)
1.1	1	1866.57	22.89
2.1	2	1872.79	56.76
3.1	3	1872.79	122.24
4.1	4	1866.57	157.11
5.1	5	1852.03	207.32
6.1	6	1800.40	264.72
7.1	7	1800.40	275.28
8.1	8	1852.03	332.68

2.2 Cable properties

The studied cable is a six–strand wire rope with an independent wire rope core (IWRC). A cross section of the rope is shown in Figure 2.2.1. In this kind of rope the outer wires of an individual strand are helically laid either opposite to (Regular Lay), or in the same direction as (Lang's Lay) the lay of the strands in the rope. Another important type of wire rope is the spiral strand, see Figure 2.2.1. The spiral strand is torque balanced but it cannot resist tension–tension fatigue as well as a six–strand wire rope wich has the same breaking load.

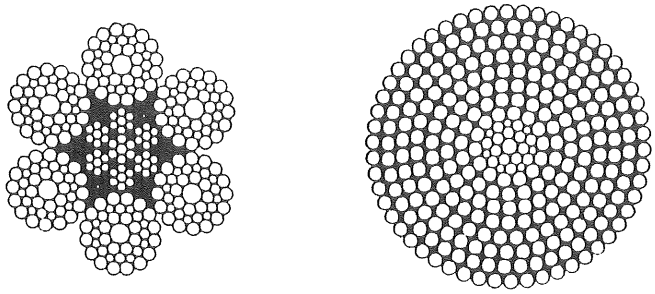

Six–strand rope (IWRC) Spiral strand

Figure 2.2.1 Cross–sections of typical wire ropes.

The wire rope is a redundant structure, i.e. the failure of a few wires does not affect the overall strength. This fact is due to the close contact of the wires, which results in friction and a good distribution of forces. The close contact may, however, cause fretting at points where two wires with different directions meet. Such inter–wire point contacts are frequent between the outer wires in the strands, and the core of a six strand wire rope. It is believed that fatigue cracks are initiated at these point contacts within the rope (Husein and Cottis, 1986). Corrosion accelerates this process and the use of lubricants slows it down.

The six strand wire rope studied is modelled with the following properties.

Diameter	76 mm
Breaking load, UBL	4290 kN
Mass per unit length	24.7 kg/m
Effective E–modulus, E	$7 \cdot 10^{10}$ N/m^2
Drag coefficient parallel to the rope, C_{DT}	0.1
Drag coefficient normal to the rope, C_{DN}	1.0
Added mass coefficient parallel to the rope, C_{MT}	0.0
Added mass coefficient normal to the rope, C_{MN}	1.0
Friction coefficient at the bottom, C_{FR}	1.0

In some test reports the breaking load is the minimum breaking load (MBL) catalogued by the manufacturer for the kind of rope that has been tested. Other test reports refer to an actual or ultimate breaking load (UBL), measured on samples of the same rope which has been fatigue tested. The UBL values are usually about 10–15% higher than the MBL values. In this study the load ranges are expressed as percentage of UBL.

The effective E–modulus consists of two parts. One part can be attributed to the elastic (bending, torsional, or axial) stiffness of the wires. The other part can be attributed to the cable geometry, such as the helix angle and the helix radius. The elastic stiffness decreases with time, while the geometric stiffness increases owing to seating of the strands and compression of the core. The effective E–modules of an old wire rope of this type can be 30–40% higher than the value tabulated above.

Correct values of the hydrodynamic parameters are difficult to find, e.g. the drag coefficient may increase considerably for a stretched cable in a current, due to the high–frequency shedding of vortices (Palo et al, 1983).

In order to assess the fatigue performance of a wire rope some additional definitions have to be made. In this study, fatigue failure is defined as a failure that results from loading the cable with a fluctuating axial load. Internal wear and fretting at point contacts between wires are thereby included in the definition of fatigue.

A limited number of fatigue tests have been performed on large diameter wire ropes. The results differ considerably, which is to some extent due to a lack of detailed, generally applied test specifications (i.e. how the cable terminations should be socketed, when a sample is to be considered as failed, etc.). The results from fatigue test results are described in S–N diagrams. If a sample fails after N load–cycles of range S, then the value (S,N) is plotted on the diagram. A curve fitting is then performed using all the plotted values, and an S–N curve for the wire rope is obtained. It is often assumed that the S–N curve follows the equation

$$\log N = \log K - m \log S, \qquad (2.2.1)$$

e.g. (DnV, 1985), (Wirsching and Light 1980). In MTD (1988) an S–N curve is derived from a number of tension–tension fatigue tests of six–strand wire ropes with IWRC. This S–N curve is chosen as the sample S–N curve. The curve is shown in Figure 2.2.2. and chosen as the sample S–N curve.

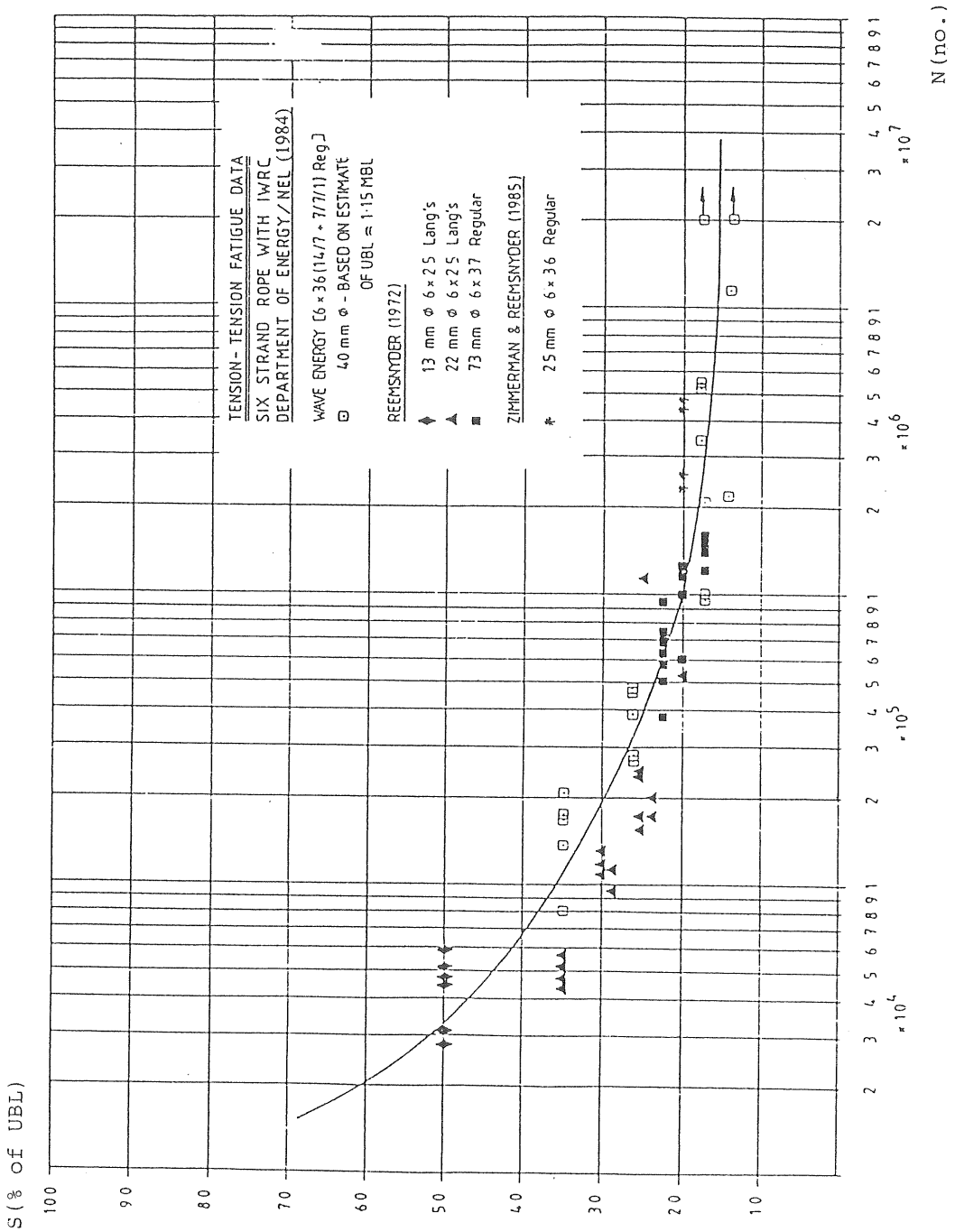

Figure 2.2.2 S–N data and an S–N curve reported in MTD (1988).

3 TIME DOMAIN SOLUTION

3.1 Establishing the static equilibrium

The forces considered to be constant within each sea–state are the wind force, the current force, the wave drift force and the thruster force. These are discussed below and their combined effect on the cables is expressed as a static cable forces necessary to keep the system in equilibrium. The tables below show results for a limited number of sea–states. These sea–states are used to model the environment of the sample problem (see also Section 7.6). Direction is denoted either by

θ , which indicates direction relative to the heading of the platform; or

θ_c , which indicates from which compass direction the wind or the waves come.

In the sample problem the directions are related by

$$\theta = 5\pi/4 - \theta_c \qquad (3.1.1)$$

Wind force

The wind force is calculated according to an ordinary drag expression,

$$F_w = \frac{1}{2} C_{Dw} \rho A_w U_{10}^2 \qquad (3.1.2)$$

where

C_{Dw} is a shape coefficient determined by windtunnel tests (Consafe, 1982),

ρ_a is the density of the air,

A_w is a characteristic area,

U_{10} is the velocity of the wind 10 m above the water surface.

Current force

The tidal current is uncorrelated to the wind driven current. Sometimes it acts in the same direction as the wind driven current, sometimes it acts in the opposite direction. For this study of the effect of the environmental force over a long period of time, the tidal current force is set to zero for all weather situations.

The wind driven current force is calculated with a drag expression corresponding to Eq. (3.1.2) where the drag coefficients were determined by wind tunnel tests (Consafe, 1982). The direction of the current force is set to $\pi/4$ rad cum sole to the direction of the wind force, according to the Ekman spiral (Dietrich and Kalle, 1965). The current speed is set to 3% of the wind speed, which is twice the value given as a rule of thumb in Dietrich and Kalle (1965).

Wave drift force

Wave drift force coefficients are calculated for regular waves with the diffraction model (Appendix 1). For each sea–state the wave drift force is calculated as

$$F_d = \sum_{i=1}^{N} D(f_i)\, S(f_i)\, \Delta f \qquad (3.1.3)$$

where

$D(f_i)$	is the wave drift force coefficient for frequency f_i
$S(f_i)$	is the value of the spectral density for frequency f_i
N	is the number of frequencies for which the wave drift force coefficients are calculated
Δf	is the interval between two successive frequencies, f_i and f_{i+1}

Thruster force and stand–off position

The platform is equipped with 4 azimuth thrusters, each of the power of 2400 kW which corresponds to a maximum force of 400 kN. When all the thrusters are run, the capacity of the power supply results in a reduction of the maximum thruster force to 320 kN.

The thrusters are used when there is a risk that the reaction force in one of the cables will reach 1/3 of the breaking load. When the platform motion becomes too large for operation, the platform is moved to the stand–off position, some 100 metres away from the installation.

The thrusters are not supposed to be needed for any of the studied sea–states. However, the platform is taken to the stand–off position for some of the worst sea–states, according to Table 3.1.5.

Total environmental force

The total environmental force is calculated as the vector sum of the wind, current, and wave drift force. The total environmental force is considered to be static within each sea–state.

Static cable forces

The cable forces needed to keep the platform in equilibrium position are calculated with STANAFAS (Avedal and Erikson, 1983). The input to these calculations are the total environmental forces, the geometry (Chapter 2.1), and the cable properties (Chapter 2.2). The results are tabulated below.

Table 3.1.1 Wind force and wind force direction relative to platform associated with the sea–states.

Sea–state			F_w	
H_s(m)	U_{10}(m/s)	Direction θ_c(deg.)	Amplitude (kN)	Direction θ (deg)
7.8	24	360	508	225
		300	605	285
		240	471	345
8.3	24	360	508	225
		300	605	285
		240	471	345
8.8	25	360	553	225
		300	646	285
		240	516	345
9.3	26	360	591	225
		300	692	285
		240	552	345
9.8	27	255	619	330
10.3	27	255	619	330
10.8	27	255	619	330
11.3	29	240	666	345
11.8	31	270	805	315
12.3	32	270	868	315

Table 3.1.2 Current force and current force direction relative to platform associated with the sea–states.

Sea–state			Current force	
H_s(m)	U_{10}(m/s)	Direction θ_c(deg.)	Amplitude (kN)	Direction θ (deg.)
7.8	24	360	144	180
		300	248	240
		240	263	300
8.3	24	360	144	180
		300	248	240
		240	263	300
8.8	25	360	154	180
		300	261	240
		240	278	300
9.3	26	360	164	180
		300	300	240
		240	304	300
9.8	27	255	364	285
10.3	27	255	364	285
10.8	27	255	364	285
11.3	29	240	380	300
11.8	31	270	475	270
12.3	32	270	501	270

Table 3.1.3 Wave drift force and wave drift force direction relative to platform associated with the sea–states.

Sea–state				F_d	
H_s(m)	T_p(s)	U_{10}(m/s)	Direction θ_c(deg.)	Amplitude (kN)	Direction θ (deg.)
7.8	12.0	24	360	70	214
			300	113	259
			240	57	345
	15.0	24	360	44	214
			300	71	259
			240	35	345
8.3	12.0	24	360	89	214
			300	143	259
			240	72	345
	16.0	24	360	47	214
			300	76	259
			240	38	345
8.8	13.0	25	360	89	214
			300	144	259
			240	72	345
	17.0	25	360	52	214
			300	84	259
			240	42	345
9.3	12.5	26	360	129	214
			300	208	259
			240	104	345
	15.5		360	76	214
			300	123	259
			240	61	345
9.8	14.0	27	255	97	319
	17.0		255	63	319
10.3	16.0		255	69	319
10.8	14.0		255	140	319
	17.5		255	83	319
11.3	16.0	29	240	151	345
11.8	16.5	31	270	132	304
12.3	16.5	32	270	161	304

Table 3.1.4 Total environmental force and force direction relative to platform associated with the sea–states.

Sea–state				Total environmental force	
H_s(m)	T_p(s)	U_{10}(m/s)	Direction θ_c(deg.)	Amplitude (kN)	Direction θ (deg.)
7.8	12.0	24	360	688	215
			300	910	270
			240	738	–30
	15.0	24	360	662	215
			300	869	270
			240	717	–30
8.3	12.0	24	360	707	215
			300	940	270
			240	752	–29
	16.0	24	360	665	215
			300	874	271
			240	719	–30
8.8	13.0	25	360	760	215
			300	991	270
			240	809	–29
	17.0	25	360	723	215
			300	933	271
			240	780	–30
9.3	12.5	26	360	845	215
			300	1132	271
			240	897	–29
	15.5	26	360	792	215
			300	1049	270
			240	855	–29
9.8	14.0	27	255	1010	–46
	17.0		255	976	–46
10.3	16.0	27	255	982	–46
10.8	14.0		255	1053	–46
	17.5		255	996	–46
11.3	16.0	29	240	1118	–29
11.8	16.5	31	270	1321	–61
12.3	16.5	32	270	1433	–61

Table 3.1.5 Static cable forces associated with the sea–states.

so = Equilibrium at stand off position

Sea–State				Cable No/ Static cable force (kN)							
H_s(m)	T_p(s)	U_{10}(m/s)	Direction θ_c(deg.)	1	2	3	4	5	6	7	8
7.8	12.0	24	360	470	680	260	190	210	220	160	290
			300	420	520	550	460	90	90	90	160
			240	180	570	530	450	630	180	210	170
	15.0		360	460	670	260	190	210	230	160	290
			300	410	500	530	450	90	90	90	160
			240	180	570	520	450	620	180	210	170
8.3	12.0		360	540	660	270	260	220	240	150	330
			300	430	550	570	470	90	80	110	160
			240	170	550	520	460	620	160	210	150
	16.0		360	500	670	240	220	250	220	160	290
			300	400	520	550	460	90	80	120	160
			240	170	550	510	440	610	160	210	150
8.8	13.0	25	360	480	720	260	180	200	220	160	300
			300	450	570	590	500	90	90	110	160
			240	180	580	560	490	660	180	210	170
	17.0		360	480	700	260	180	200	220	160	290
			300	420	540	570	480	90	80	110	160
			240	180	580	550	480	650	180	210	170
9.3	12.5	26	360 so	590	610	590	370	310	120	260	830
			300 so	490	540	890	540	140	110	130	390
			240 so	310	280	690	540	530	260	150	160
	15.5		360	520	710	240	220	190	210	160	280
			300	370	400	420	430	100	350	390	170
			240	160	560	580	470	660	170	190	160
9.8	14.0	27	255 so	240	670	590	590	730	110	130	230
	17.0		255	120	730	730	330	660	190	110	120
10.3	16.0		255	120	730	740	330	660	190	110	120
10.8	14.0		255 so	230	790	580	610	800	130	130	230
	17.5		255	120	730	750	330	660	190	110	120
11.3	16.0	29	240 so	200	490	570	690	770	120	140	210
11.8	16.5	31	270 so	290	660	820	660	460	90	110	190
12.0	16.5	32	270 so	290	690	880	700	450	90	100	190

3.2 Motion owing to the first order wave force

In the study, waves are simulated according to the following equation.

$$\zeta(t) = \mathrm{Re}\ \{\zeta c(t)\},$$

$$\zeta_c(t) = \sum_{i=0}^{N/2} \zeta_{ci}(t) \qquad (3.2.1)$$

$$\zeta_{ci}(t) = \eta_i e^{j(2\pi f_i t + \psi_i)}$$

where

$\zeta(t)$	is the wave elevation as a function of time,
η_i	is the amplitude of component no. i,
f_i	is the frequency of component no. i,
ψ_i	is a random phase angle of component no. i,
N/2+1	is the number of components.

The frequencies of the components are defined as

$$f_i = f_0 + i\Delta f \quad , i=0,1,2,....,N/2 \qquad (3.2.2)$$

where

f_0	is the lowest frequency for which the hydrodynamic properties were calculated in the diffraction model (Appendix 1).
Δf	= 1/T, where T is the time length of the simulated wave
N/2	= $(f_2-f_0)/\Delta f$, where f_2 is the highest frequency for which the hydrodynamic properties were calculated in the diffraction model. (f_0=0.0366Hz and f_2=0.145Hz in the solution of the sample problem.)

The amplitude η_i is a function of the spectral density or "wave–spectrum", $S(f_i)$.

$$\eta_i = (2S(f_i)\Delta f)^{1/2} \qquad (3.2.3)$$

$S(f_i)$ is defined in Chapter 5.

The phase angles, ψ_i, are samples from a random variable with the probability density function $p(\psi_i)$,

$$p(\psi_i) = \begin{cases} 1/2\pi\,, & 0 < \psi_i \leq 2\pi \\ 0\,, & \text{otherwise} \end{cases} \qquad (3.2.4)$$

The sea surface is generally assumed to be a realization of a Gaussian process. Eq. 3.2.1 represents a Gaussian process only in the limit $N \to \infty$. Elgar et al (1985) assume that one thousand components is enough for most applications. In the study 430 components in the range 0.037 Hz to 0.145 Hz is used. The error that may arise from this limitation is assumed to be small.

The structure's response to the wave (Eq. 3.2.1) is computed by use of the principle of superposition.

$$x_k(t) = \sum_{i=0}^{N/2} T_{ik}\, \zeta_{ci}(t) \quad ,k = 1,2,...6 \qquad (3.2.5)$$

where

k	indicates degree of freedom,
$x_k(t)$	is the complex motion,
ζ_{ci}	is the i'th complex wave component (see Eq. 3.2.1),
T_{ik}	is the transfer function between the i'th wave component and the platform motion in the k'th degree of freedom:

$$T_{ik} = \hat{T}_{ik}\, e^{j\phi_{ik}} \qquad (3.2.6)$$

To establish the equation of motion, from which the transfer function T_{ik} can be found, results from calculations with the diffraction model (Appendix 1) are used. The diffraction model does not take into account the damping effect of viscosity. This effect has to be included in this study, however, because realistic amplitudes of the transfer function near eigenfrequencies are needed. Therefore, a simple model of the viscous damping in heave (3rd degree of freedom) is included by a force, F_{vi3}, proportional to the relative velocity squared. For each component i the equation of motion has the following form.

$$(\underline{\underline{m}} + \underline{\underline{a}}_i)\, \ddot{\underline{x}}_i + \underline{\underline{b}}_i\, \dot{\underline{x}}_i + \underline{\underline{c}}\, \underline{x}_i = \underline{F}_{ei}\, \frac{H_s}{2} + \underline{F}_{vi} \qquad (3.2.7)$$

where

$\underline{\underline{m}}$ is the mass matrix for the platform,

$\underline{\underline{a}}_i$ is the added mass matrix, interpolated from the diffraction model results,

$\underline{x}_i$ is a vector containing the motion in the six degrees of freedom,

$\underline{\underline{b}}_i$ is the radiation damping matrix, interpolated from diffraction model results,

$\underline{F}_{vi}$ is a vector expressing the effect of viscosity in heave (or 3rd degree of freedom) motion. The only non–zero component of the vector is the viscous damping force in heave:

$$F_{vi3} = \frac{1}{2} C_{D3} \rho_w A(\dot{\zeta}_{ci} - \dot{x}_{i3}) |\dot{\zeta}_{ci} - \dot{x}_{i3}| \qquad (3.2.8)$$

C_{D3} is a drag coefficient determined by model tests,

ρ_w is the water density,

A is the platform area normal to the heave direction,

$\dot{x}_{i3}$ is the platform velocity in heave,

$\underline{\underline{c}}$ is the stiffness matrix,

$\underline{F}_{ei}$ is a vector containing the wave exciting forces per unit of wave amplitude in the six degrees of freedom, calculated with the diffraction model,

H_s is the significant wave height calculated from the applied wave–spectrum,

$\dot{}$ and $\ddot{}$ indicate the first and second time derivative.

From the solution to Eq. 3.2.7 the transfer function is calculated as

$$\hat{T}_{ik} = \frac{|x_{ik}|}{H_s/2}, \quad k = 1,2,...6,$$
$$i = 0,1,2,...N/2 \qquad (3.2.9)$$

ϕ_{ik} = phase angle of x_{ik}.

The use of a quadratic term, F_{vi3} ,when calculating transfer functions for use in the linear superposition (Eq. 3.2.5), is not mathematically stringent. The solutions to Eq. 3.2.7 near the eigenfrequencies are to be seen as rough estimates that take into consideration the effect of damping and the varying magnitude of the damping with respect to the relative water velocity. Figure 3.2.1 is a comparison between calculations with and without the damping term. The figure also shows model test results reported in Consafe group (1982).

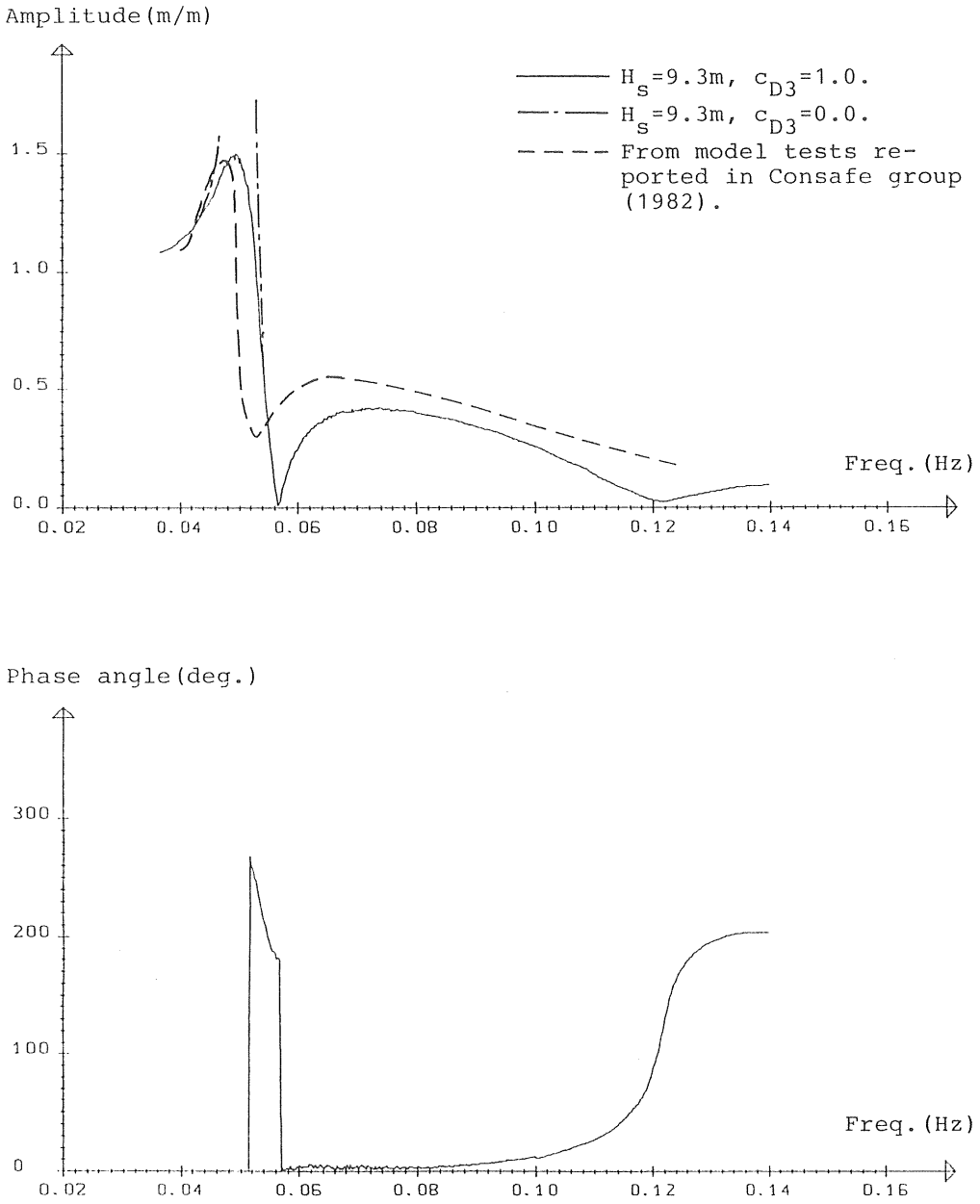

Figure 3.2.1 Transfer functions from wave to heave motion.

3.3 Calculation of the cable load

The cable load is calculated as a function of time using MODEX. MODEX is a dynamic model based on a finite element discretization of the cable (see Figure 3.3.1). The cable is regarded as a long slender structure with negligible shear forces and moments. The model has been extensively tested (see Section 1.1).

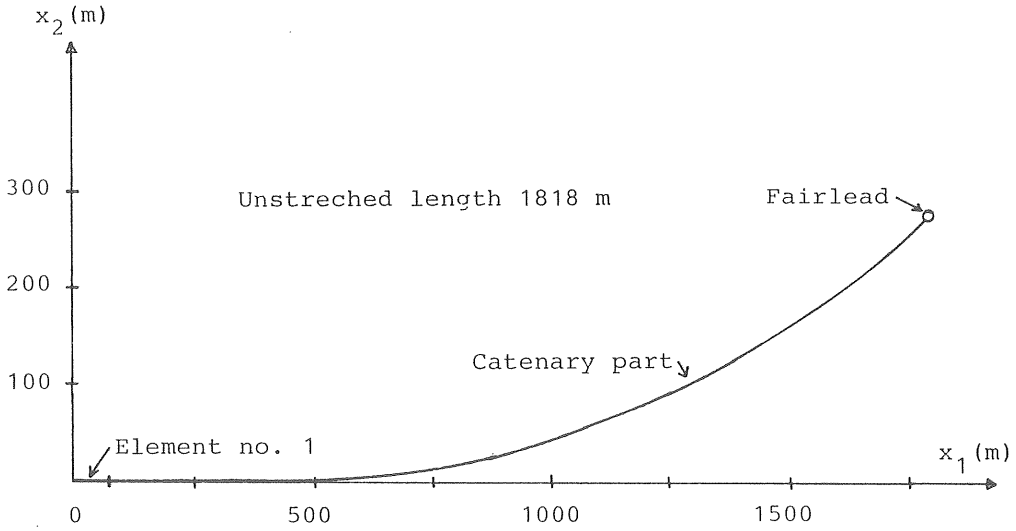

Figure 3.3.1 Static configuration of cable no. 2 calculated for the sea–state associated with H_s = 7.8 m, T_p = 12.0 s, $\theta_c = 360^0$.

In the solution for the sample problem the load is calculated for the catenary part. The number of finite elements is 20, which is considered to be an appropriate value with respect to computer time and accuracy. The influence of the number of finite elements on the response is analysed in the parameter study.

The cable load is evaluated for the catenary part of the cable. The difference in mean–load between different elements is small. However, the amplitudes of the load fluctuations may vary. It is believed that the catenary part will experience the largest load fluctuations.

The platform motion is transformed to fairlead motion according to Appendix 3 with a timestep of 0.15 s. In MODEX the timestep is required to be about ten times shorter in order to obtain stable solutions. A cubic spline function is used to interpolate input values to MODEX from the time history of fairlead motion.

In MODEX the Morison equation is applied for the calculation of surface forces and volume forces. The drag coefficients and the added–mass coefficients are assumed to be constant and the water current is assumed to be stationary. The influence of a variation of these parameters on the response is low (see Chapter 6).

4. ENVIRONMENTAL FORCES

Wind, waves and current are the three phenomena to be considered. Their inter-dependence is complicated and random. However, in this study the variation of the weather is based only on the distribution of wave–spectra, and simple deterministic relations are applied between wave–spectrum and wind, as well as between wind and current. The simplification is motivated by the assumption that the ranges of the load–cycles generated by the environment are mainly a function of the first order wave and the cable mean–load.

4.1 The concept of sea–state

The nature of the wave climate is such that it can be assumed to be a stationary process, when studied over shorter time periods (e.g. 3 hours). These stationary processes are called "sea–states" in the report, and they are represented by wave–spectra. In the present study the wave–spectra are of the JONSWAP form and the input to the simulations are the significant wave height H_s, the spectral peak period T_p, and the direction of the wind and the waves θ_c. The distribution of sea–states over longer time periods (e.g. 1 year) can be represented by historical observations and measurements. At Haltenbanken, measurements of the wave profiles and the wave directions were made from 1980 to 1986, at a rate of about one measurement every three hours. Scatter diagrams for H_s, T_p and θ_c evaluated from these measurements, are used in the study as a representation of the long term distribution of sea–states at the sample location (see Appendix 4).

4.2 Choice of wave–spectrum

The wave–spectrum used is the JONSWAP model:

$$S(f) = \alpha g^2 (2\pi)^{-4} f^{-5} \exp\left(-\frac{5}{4}\left(\frac{f}{f_m}\right)^{-4}\right)\gamma^{\exp\left(-\frac{(f-f_m)^2}{2\sigma^2 f_m^2}\right)} \qquad (4.2.1)$$

$$\sigma = \begin{cases} 0.07, & f \le f_m \\ 0.09, & f > f_m \end{cases}$$

where

f_m is the spectral peak frequency,

$f_m = 1 / T_p$

σ, α, γ relate to the shape of the spectrum.

This spectrum is a modified Pierson Moskowitz spectrum that can take into account the effect of fetch restrictions and sea–states that have the wave energy concentrated within a narrow frequency range.

The JONSWAP model was developed during the "Joint North Sea Wave Project", a major study of the wave climate off the island of Sylt, by Hasselman, K, et al (1973). Here, the choice of parameter values (Table 4.3.1) is based on the fitting of 115 empirical spectra from measurements off the Norwegian coast at Famita, Utsira, Statfjord, and Halten, to the JONSWAP model (Houmb and Overvik, 1976).

A comparison between the JONSWAP model and analyses of wave measurements at Utsira 1981, performed by Houmb and Øyan (1981), shows that the model underestimates the high frequency tail of the empirical spectra. In their report, Houm and Øyan discuss the parameter γ, which expresses the peakedness of the spectrum. It is expected that γ tends to unity (PM spectrum) for fully arisen seas. Houmb and Øyan therefore recommend small γ values, say less than 3 for extreme sea–states in northern waters.

4.3 Relations between wind, waves and current

During the "Joint North Sea Wave Project" the spectral parameters of the JONSWAP model were related to the physical situation (wind, fetch etc) that generated the measured waves. From these observations the following equation, that relates the wind velocity to the spectral parameters, was derived by Houmb and Overvik (1976).

$$f_m = 0.1086\, U_{10}^{0.32}\, H_s^{-0.66} \qquad (4.3.1)$$

where

f_m is the frequency of the spectral peak

U_{10} is the wind velocity 10 m above the sea surface,

H_s is the significant wave height evaluated from the spectral density function.

This equation indicates that the wind velocity is not only associated with the wave height, but also with the average wave period. However, in the present study the wind velocities were only determined roughly, by comparing frequency tables from Haltenbanken of wind velocities and significant wave heights from 1980 to 1986 (OCEANOR 1987). These wind velocities are shown in Table 4.3.1.

The velocity of the wind driven current is set to 3% of the velocity of the wind. The direction of the wind driven current is set to $\pi/4$ rad cum sole to the wind direction, according to the Ekman spiral (Dietrich and Kalle, 1965). The tidal current is not taken into account.

Table 4.3.1. Values on the JONSWAP parameters and the associated wind velocity.

Sea–state		JONSWAP		U_{10}(m/s)
H_s(m)	T_p(s)	α	γ	
7.8	12.0	0.0082	4.58	24
	15.0	0.0046	2.21	24
8.3	12.0	0.0091	4.82	24
	16.0	0.0042	2.10	24
8.8	13.0	0.0077	4.51	25
	17.0	0.0041	1.52	25
9.3	12.5	0.0099	4.94	26
	15.5	0.0053	2.98	26
9.8	14.0	0.0072	4.35	27
	17.0	0.0044	2.34	27
10.3	16.0	0.0049	3.34	27
10.8	14.0	0.0085	4.69	27
	17.5	0.0047	2.40	27
11.3	16.0	0.0058	3.75	29
11.8	16.5	0.0058	3.75	31
12.3	16.5	0.0063	4.02	32

5 SPECTRAL ANALYSIS

In this report spectral analysis is used for two purposes. The first is to simulate the platform motion from wave–spectra. The second is to analyse the resulting cable load time histories. The description below of how the spectral parameters are defined in this report follows a description of spectral methods given in Press et al (1986).

Fourier transform

A complex signal h(t) in the time domain may be represented in the frequency domain by a Fourier transform. Define a function of frequency H(f) by

$$H(f) = \int_{-\infty}^{\infty} h(t) e^{2\pi i f t} dt, \qquad (5.1)$$

then h(t) can be found from H(f) by

$$h(t) = \int_{-\infty}^{\infty} H(f) e^{-2\pi i f t} df, \qquad (5.2)$$

H(f) is the Fourier transform of h(t).

From a finite number of sampled points of h(t),

$$h_k \equiv h(t_k), \qquad (5.3)$$

where

$t_k \equiv k\Delta t, \quad k=0, 1, 2, \ldots N-1,$
Δt is the time increment,
N is an even integer;

an approximation of the Fourier transform (Eq. 5.1) can be found by a discrete sum;

$$H(f_n) \approx \Delta t \sum_{k=0}^{N-1} h_k e^{i2\pi kn/N}, \quad f_n = \frac{n}{N\Delta t}, \quad n = -\frac{N}{2}, \ldots \frac{N}{2} \qquad (5.4)$$

or,

$$H(f_n) \approx \Delta t H_n \qquad (5.5)$$

where

$$H_n \equiv \sum_{k=0}^{N-1} h_k e^{i2\pi kn/N}, \qquad n = -\frac{N}{2},\ldots\frac{N}{2} \tag{5.6}$$

H_n is called the discrete Fourier transform of the N points h_k.

Eq. 5.6 is periodic in n, with period N ($H_{-n} = H_{N-n}$, n=1,2,..). It is therefore convenient to let the n in H_n vary from 0 to N–1 (one complete period). This convention, which is followed in many numerical solution routines, means that

$f = 0$	corresponds to	$n = 0$,
$0<f<f_c$	corresponds to	$1 \le n \le (N/2)-1$,
$-f_c<f<0$	corresponds to	$(N/2)+1 \le n \le N-1$ and
$f = \pm f_c$	corresponds to	$n = N/2$.

f_c is the Nyquist critical frequency, given by

$$f_c \equiv \frac{1}{2\Delta t}. \tag{5.7}$$

If the series h_k is real then the Fourier transform coefficients H_n have the following symmetrical properties

$$\begin{aligned} &\text{Re}\,\{H_{N-n}\} = \text{Re}\,\{H_n\}, \quad n = 1, 2, \ldots, \frac{N}{2} \\ &\text{Im}\,\{H_{N-n}\} = -\text{Im}\,\{H_n\}, \quad n = 1, 2, \ldots, \frac{N}{2}-1 \\ &\text{Im}\,\{H_o\} = \text{Im}\,\{H_{N/2}\} = 0 \end{aligned} \tag{5.8}$$

The formula which recovers the series h_k exactly from the Fourier transform coefficients H_n is called the inverse Fourier transform. The inverse Fourier transform can be written

$$h_k = \frac{1}{N}\sum_{n=0}^{N-1} H_n\, e^{-i2\pi kn/N} \tag{5.9}$$

Spectral density

The total energy in a signal h(t) can be computed in either the time domain or the frequency domain;

$$\text{Total energy} \equiv \int_{-\infty}^{\infty} |h(t)|^2 dt = \int_{-\infty}^{\infty} |H(f)|^2 df. \qquad (5.10)$$

A function that shows the distribution of energy over frequency is called a spectral density function. In the report a one sided (i.e. defined only for positive frequencies) spectral density function, with the following definition, is used.

$$P_h(f) = |H(f)|^2 + |H(-f)|^2, \quad f \geq 0 \qquad (5.11)$$

or, when h(t) is a real function,

$$P_h(f) = 2|H(f)|^2, \qquad f \geq 0 \qquad (5.12)$$

The total energy is then the integral of $P_n(f)$ from f = 0 to f = ∞. The total energy and the spectral density will, in general, be infinite (there are no limits of t in Equation (5.1)). It is therefore practical to use the spectral density per unit time, which is found by computing the spectral density from a finite representative stretch of h(t) and then dividing the result by the lenght of the stretch.

A discrete estimate of the spectral density of a real function h(t) per unit time using values h_k , sampled according to Equation 5.3,is

$$S_n = \begin{cases} \frac{1}{N^2} |H_n|^2, & n = 0 \text{ and } N/2 \\ \frac{2}{N^2} |H_n|^2, & n = 1,2,...(N/2)-1, \end{cases} \qquad (5.13)$$

The relation between S_n, the mean squared amplitude of h(t) and the mean squared amplitude of h_k is

$$\frac{1}{T}\int_0^T |h(t)|^2 dt \approx \frac{1}{N}\sum_{k=0}^{N-1} |h_k|^2 = \sum_{n=0}^{N/2} S_n \qquad (5.14)$$

In the present report the frequency increment, Δf, is constant and a continuous spectral density of h(t), S(f), is defined from the discrete spectral density, S_n, for the frequencies f_n:

$$S(f_n) = S_n \cdot \frac{1}{\Delta f} \qquad (5.15)$$

where

$$f_n = \frac{n}{N\Delta t}, \quad n = 0, 1, 2, \ldots \frac{N}{2}$$

$$\Delta f = \frac{1}{N\Delta t}$$

The moments, m_i, of the spectral density $S(f_n)$ are defined

$$m_i = \sum_{k=0}^{N/2} S(f_n) f_n^{\,i} \Delta f \qquad (5.16)$$

Spectral Filtering

Consider a real time series

$$h_k, \quad k = 0, 1, \ldots, N-1,$$

translated in such a way that

$$h_0 = 0, \text{ and } h_{N-1} = 0.$$

From the Fourier transform H_n of this series a transform H_n', filtered at $f=f_f$, is defined as

$$H_n' = \begin{cases} H_n, & \text{for components that correspond to frequencies } f<f_f, \\ (\mathrm{Re}(H_n), 0), & \text{for the component that corresponds to } f=f_f, \\ (0, 0), & \text{for components that correspond to } f>f_f. \end{cases}$$

An inverse Fourier transform h_k' of H_n' will then be a filtered version of h_k. This way to filter is recommended in Press et al. (1987). For more details, see for example Brigham (1974).

The parameter study in Chapter 6 shows that the contribution to the fatigue damage from frequency components higher than $2 \cdot f_2$, where f_2 is the highest first order wave frequency (see Equation 3.2.2), is negligible. The filter frequency f_f is therefore chosen to $2 \cdot f_2$.

6 PARAMETER STUDY

This chapter is a study of how the "output", i. e. the cable load time history, changes with respect to variations of the "input" and the "model". The sea–state, defined by a first order wave–spectrum, together with an incoming wave direction, a current velocity, and a cable configuration, corresponding to a static cable force, is regarded as the "input". The "model" consists of the mathematical models of the platform and the cable. The "output" is characterized by a fatigue damage value and a spectrum calculated from the cable load time history. The following "input" and "model" parameters are studied.

Table 6.1 The "input" parameters and their basic values.

"Input" parameter	Basic value
Significant wave height, H_s	9.3 m
Spectral peak period, T_p	14.3 s
Incoming wave direction relative to platform, θ	270 deg
Cable mean–load, $\bar{P}$	915 kN
Current velocity, v_c	1.0 m/s

Table 6.2 The "model" parameters and their basic values.

"Model" parameter	Basic value
Viscous damping coefficient for platform motion in heave, C_{D3}	1.0
Viscous damping coefficient for cable motion in normal direction, C_{DN}	1.0
No. of finite elements in cable model, n_{el}	20
Studied finite element	no. 15
Effective E–modulus for cable, E	$7.0 \cdot 10^{10}$ N/m^2
Ultimate breaking load, UBL	4290 kN
S–N curve	(Fig. 2.2.2)

Only one "input" or "model" parameter is varied at a time. For each variation three one hour (real time) simulations are performed. The characteristics of the cable load spectrum are calculated as averages from these three simulations. However, the only characteristic that shows any significant difference from simulation to simulation (within each variation) is the fatigue damage (see Table 7.2.1).

Different H_s and T_p are modelled by altering the f_m, α and γ values, the shape parameters of the JONSWAP spectrum, according to Houm and Overvik (1977, Table 23). The wave–spectra are truncated (see Equation 3.2.2). The significant wave height evaluated after truncation is called H_s' in the Table 6.3. The truncated wave spectrum is characterized by a variance, m_{0w}, a zero up–crossing period, T_{2w}, and a spectral width, ε_w;

$$\varepsilon_w = \sqrt{1 - \frac{m_{2w}}{m_{0w} \cdot m_{4w}}} \qquad (6.1)$$

$$T_{2w} = \sqrt{m_{0w}/m_{2w}} \qquad (6.2)$$

m_{iw} is the i–th moment of the spectrum.

The corresponding characteristics are also calculated for the resulting cable load spectrum, i. e. m_{0p}, T_{2p}, ε_p. The fatigue damage is obtained by direct counting of the cable force time history as is described in Section 7.1. The used S–N curve is the curve given in Figure 2.2.2.

Table 6.3 Characteristic values of the input wave–spectra.

H_s (m)	T_p (s)	$f_m(s^{-1})$	α	γ	H_s' (m)	T_{2w} (s)	ε_w
7.8	14.3	0.0699	0.0049	2.77	7.4	12.2	0.46
8.8	14.3	0.0699	0.0058	3.73	8.6	12.4	0.45
9.3	12.0	0.0833	0.0115	5.20	9.1	11.0	0.36
"	13.7	0.0730	0.0072	4.31	9.1	12.1	0.43
1)"	14.3	0.0699	0.0063	4.00	9.1	12.5	0.45
	14.9	0.0671	0.0057	3.52	9.2	12.8	0.47
"	15.8	0.0633	0.0050	2.73	9.2	12.8	0.50
"	16.6	0.0602	0.0045	2.10	9.1	13.6	0.52
	17.5	0.0571	0.0040	1.61	9.1	14.0	0.54
9.8	14.3	0.0699	0.0068	4.22	9.6	12.5	0.45
12.3	14.3	0.0699	0.0098	4.97	12.0	12.6	0.44

1) Basic values

By comparing the spectral width, ε_p, the zero up–crossing period, T_{2p}. and the variance, m_{op}, of the cable load spectrum with the corresponding values of the wave spectrum (ε_w, T_{2w}, and m_{ow}) an assessment is obtained of how the transfer of variance varies when the "input" and "model" parameters are changed.

An increase in wave height results in a decrease of the transfer of variance between the wave and the heave motion due to the non–linear damping term of the equation of motion in heave. The transfer of variance from the platform motion to the cable load will, however, increase due to the non–linear relationship between motion and cable load. The latter effect dominates, as is seen in Table 6.4 and Figure 6.1.

Table 6.4 Results for different significant wave height of input spectrum.

H_s (m)	$\varepsilon_p/\varepsilon_w$	T_{2p}/T_{2w}	m_{op}/m_{ow} ($N^2/m^2 \cdot 10^9$)	$\bar{d}$ (10^{-4}/h)
7.8	0.74	1.12	4.51	0.041
8.8	0.71	1.11	4.80	0.155
9.3	0.69	1.10	4.92	0.234
9.8	0.69	1.10	4.97	0.332
12.3	0.66	1.10	5.24	1.248

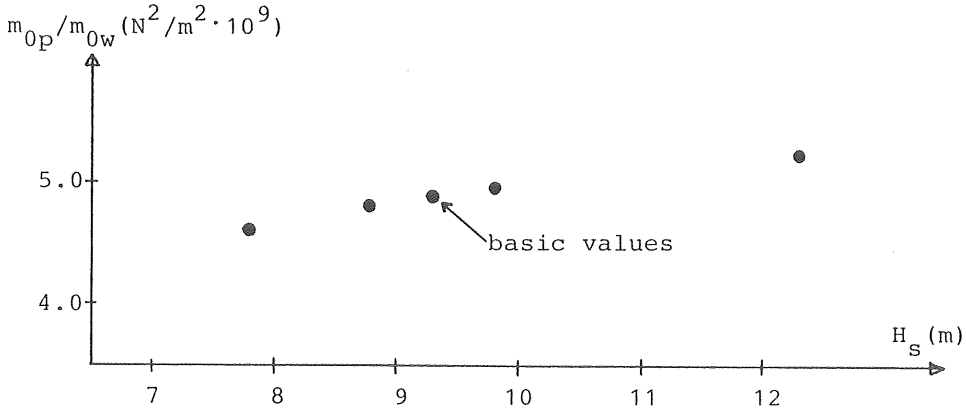

Figure 6.1 Transfer of variance for different H_s.

The eigenperiod of the platform heave motion is about 19 s. It is therefore natural that there is an increase in the transfer of variance when the dominating period, T_p, of the generating wave–spectrum approaches 19 s. This can be seen in Table 6.5 and Figure 6.2. However, there is also an important influence from the motion in other degrees of freedom, which might explain the decrease for the highest period, T_p = 17.5. The importance of the eigenmodes of the cable, the first three of which lie within 6.7 s and 11.1 s (as calculated with MODEX), are not studied explicitly.

Table 6.5 Results for different peak period of input spectrum.

T_p (s)	$\varepsilon_p/\varepsilon_w$	T_{2p}/T_{2w}	m_{op}/m_{ow} ($N^2/m^2 \cdot 10^9$)	$\bar{d}$ (10^{-4}/h)
12.0	0.78	1.10	3.42	0.051
13.7	0.70	1.12	4.57	0.199
14.3	0.69	1.10	4.92	0.234
14.9	0.70	1.11	5.02	0.246
15.8	0.72	1.10	5.08	0.230
16.6	0.75	1.11	5.09	0.211
17.5	0.78	1.10	4.98	0.195

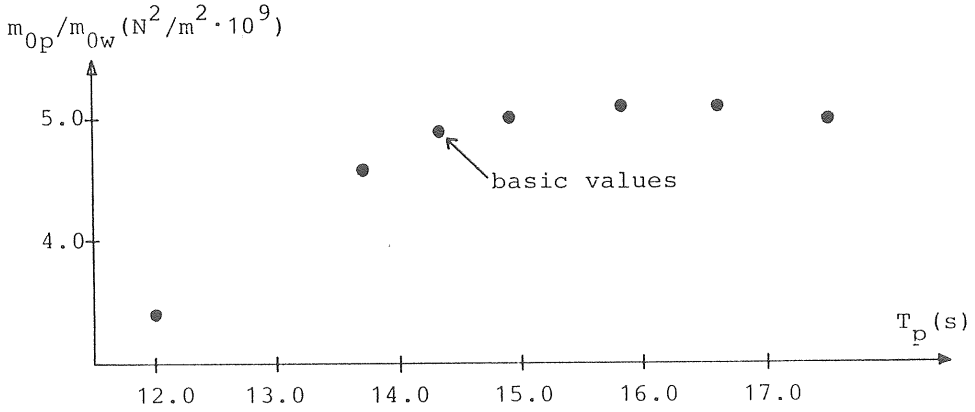

Figure 6.2 Transfer of variance for different T_p.

Tangential motions of the cable result in larger cable load fluctuations than corresponding motions in the normal direction of the cable. It would therefore have been expected that the maximum of the transfer of variance would occur when the incoming wave direction coincides with the direction of the cable. However, the maximum occurs for $\theta = 215$ degrees whereas the cable direction is 255 degrees, as can be seen in Table 6.6 and Figure 6.3.

Table 6.6 Results for different incoming wave direction relative to platform.

θ (deg)	$\varepsilon_p/\varepsilon_w$	T_{2p}/T_{2w}	m_{op}/m_{ow} ($N^2/m^2 \cdot 10^9$)	$\bar{d}$ (10^{-4}/h)
180	0.73	1.10	2.45	0.019
215	0.67	1.10	6.94	0.606
258	0.67	1.11	5.10	0.253
270	0.69	1.10	4.92	0.234
282	0.71	1.10	3.30	0.067
331	0.82	1.08	1.15	0.000

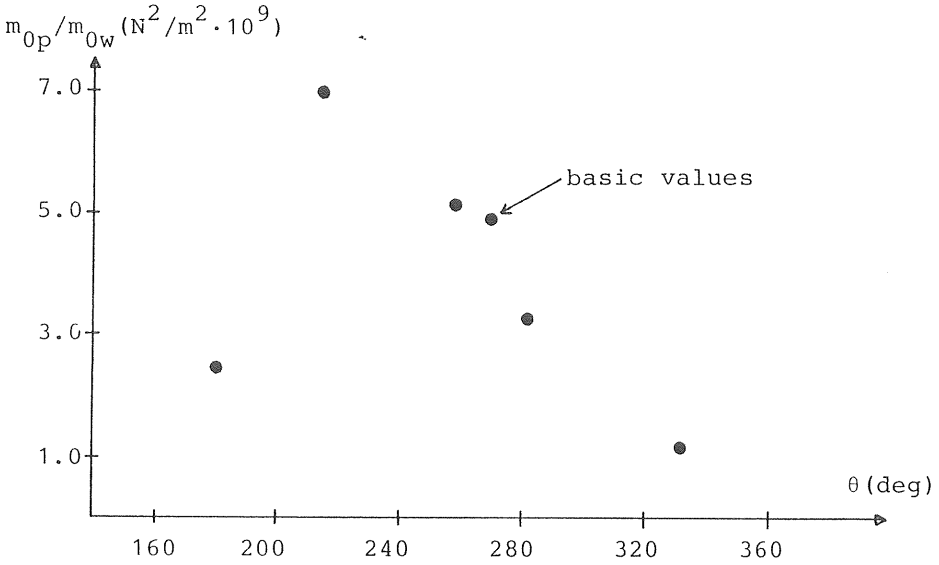

Figure 6.3 Transfer of variance for different θ.

What was said above about the non–linear relationship between cable motion and cable load is clearly underlined by Table 6.7 and Figure 6.4, which shows the increase in the transfer of variance as the cable mean–load increases.

Table 6.7 Results for different cable mean–load.

$\bar{P}$ (kN)	$\varepsilon_p/\varepsilon_w$	T_{2p}/T_{2w}	m_{op}/m_{ow} ($N^2/m^2 \cdot 10^9$)	$\bar{d}$ (10^{-4}/h)
107	1.56	0.97	0.04	0.0
298	1.16	1.06	0.79	0.0
598	0.80	1.10	3.20	0.086
663	0.78	1.10	3.64	0.119
735	0.73	1.10	4.10	0.151
835	0.69	1.11	4.63	0.203
909	0.69	1.11	4.92	0.234
985	0.69	1.11	5.20	0.267
1396	0.64	1.11	6.21	0.409

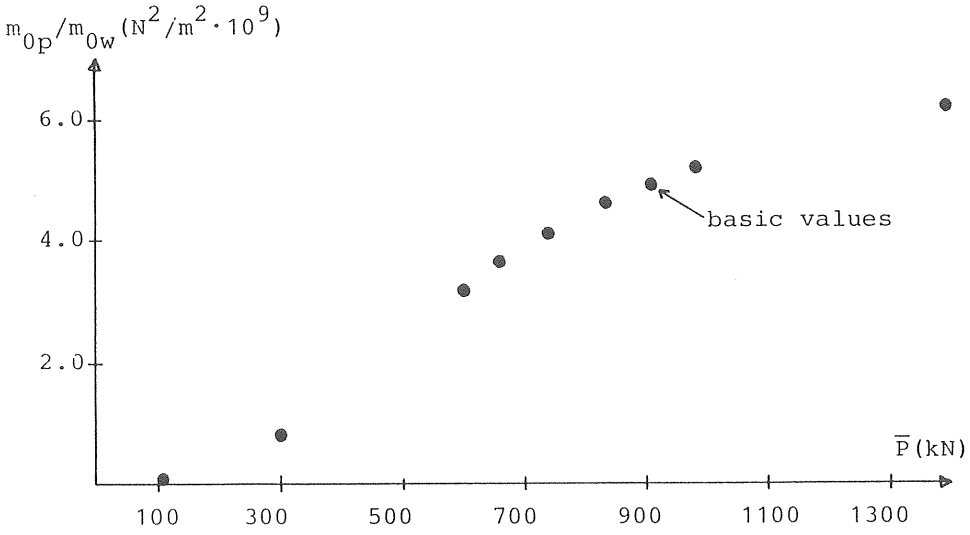

Figure 6.4 Transfer of variance for different $\bar{P}$.

Table 6.8 shows that if the viscous heave damping is ignored the fatigue damage will be overestimated. Some model of viscous heave damping should therefore be included in the calculation of the platform motion.

Table 6.8 Results for different viscous heave damping.

C_{D3}	$\varepsilon_p/\varepsilon_w$	T_{2p}/T_{2w}	m_{op}/m_{ow} ($N^2/m^2 \cdot 10^9$)	$\bar{d}(10^{-4}/h)$
0.0	0.91	1.27	9.56	1.08
1.0	0.69	1.11	4.92	0.234

The effective elasticity modulus of the cable, E, is an important parameter, as can be seen in Table 6.9. E increases with time owing to seating of the wires within the cable. A correct value of E may be hard to find.

Table 6.9 Results for different E–modula.

$E(10^{10}N/m^2)$	$\varepsilon_p/\varepsilon_w$	T_{2p}/T_{2w}	m_{0p}/m_{ow} $(N^2/m^2 \cdot 10^9)$	$\bar{d}(10^{-4}/h)$
5.0	0.69	1.11	2.59	.023
7.0	0.69	1.10	4.92	.234

As the tension–tension fatigue is a function of both the mean load (indirectly) and the range of the load–cycles, it is not obvious which element of the cable is most affected. Elements close to the fairlead experience larger mean loads than elements further down, but the cable load fluctuations close to the fairlead are smaller. Three different finite elements, nos 13, 15, and 18, are analysed in the parameter study. The results are shown in Table 6.10. Element no. 13, which is the lowest positioned of the three, is the most affected.

Table 6.10 Results for different finite elements.

Element	$\varepsilon_p/\varepsilon_w$	T_{2p}/T_{2w}	m_{0p}/m_{ow} $(N^2/m^2 \cdot 10^9)$
13	0.69	1.10	4.95
15	0.69	1.11	4.92
18	0.69	1.10	4.86

No significant difference in the results is obtained when the number of elements in the cable model, n_{el}, is varied between 16, 20, and 24.

7. METHODS OF FATIGUE CALCULATION

A statistical way of studying the fatigue of a structural component is to consider the load to which the component is subjected and the strenght of the component as two random variables that vary with time. A failure occurs when the load exceeds the strength. The time to such an exceedance is called the time to fatigue failure. In this chapter two different methods of calculation of the expected value of the time to fatigue failure are studied. The calculation of the risk of failure before the expected time is, however, not within the scope of the present report.

The methods are a method of using narrow band approximations presented by Wirsching (1980) and a method of using transfer functions between wave–spectra and cable load. Both methods are based on the concept of fatigue damage (see section 7.1) and motivated by the aim of reducing the need for simulations.

7.1 Load–cycle counting

Fatigue tests are usually performed with a fluctuating load that can be characterized by a load range, S, a mean value, $\bar{P}$, and a number of load–cycles to failure, N (Figure 7.1.1). Results from such tests are plotted on diagrams and curves are fitted to the plotted points (Figure 2.2.2). The curves are called S–N curves and show N as a function of S.

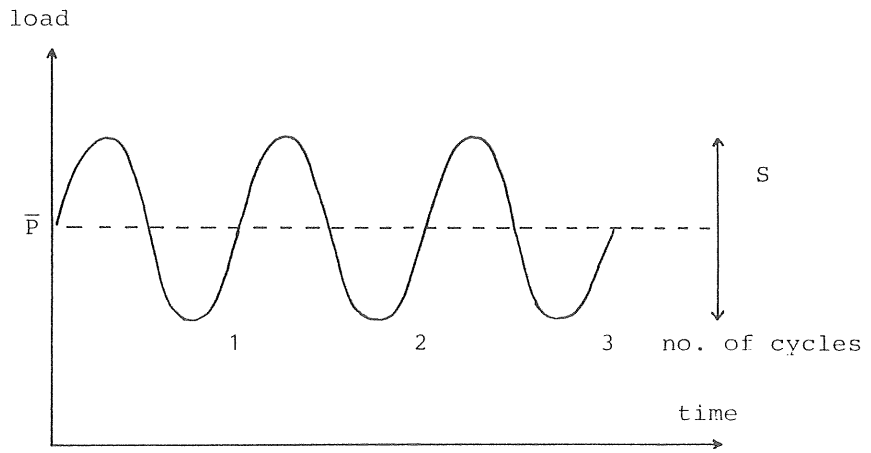

Figure 7.1.1 Definitions of fatigue load.

A cyclic load applied to a structure will change its material properties; cracks may be initiated or continue to propagate, the material may harden at crack ends due to high local stresses, etc. These changes, which may ultimately lead to failure, can be quantified using the concept of fatigue damage. The changes caused by a load (S_i, $\bar{P}_i$, n_i) are then expressed as a fatigue damage d_i:

$$d_i = d_i(S_i, \bar{P}_i, n_i).$$

It is also believed that the fatigue damage is permanent and that the fatigue damages from a sequence of different loads can be accumulated. A simple and widely accepted way of assessing the accumulated fatigue damage is to apply the linear damage rule by Palmgren and Miner. According to this rule the fatigue damage d_i, incurred by n_i cycles of the load (S_i, $\bar{P}_i$), is linearly proportional to the maximum number of cycles N_i of the same load that the material can resist before failure:

$$d_i = \frac{n_i}{N_i} \qquad (7.1.1)$$

The rule assumes that the frequency of loading (i.e. the number of cycles per time unit) and the order in which different loads are applied can be ignored. Failure is predicted to occur if

$$\sum_i d_i \geq 1 \qquad (7.1.2)$$

If an S–N curve can be obtained for the material and if the linear damage rule is applied, the problem of assessing the time to fatigue failure is reduced to a counting or a prediction of the number of cycles n_i of different loads (S_i, $\bar{P}_i$) to which the material is subjected. For a load process that has a narrow banded frequency spectrum, the number of cycles is obvious (Figure 7.1.2a). For a load process that has a wide banded frequency spectrum, the irregular load history has to be transformed to a sequence of load–cycles by the use of an algorithm of some kind (Figure 7.1.2b). One way of defining cycles from irregular load histories is the rain flow algorithm. The method of using narrow band approximations presented by Wirsching (1980) is based on the rain flow algorithm. The algorithm can be described as follows (see also Figure 7.1.3).

1. Reduce the load time history to local minima and maxima and let the time axis point downwards.

2 Draw lines between the minima and maxima and regard these lines as roofs.

3. Let flows of rain start at the inside of each minima and maxima (1,2,3,...) and then flow along the roofs.

4. Stop a flow of rain that started at a minimum when another flow falls down on it (3a and 5a) or when a minimum is encountered that is smaller than the minimum from which the flow started (1a).

5. Stop a flow of rain that started at a maximum when another flow falls down on it or when a maximum is encountered that is greater than the maximum from which the flow started (2a and 4a).

6. Define half–cycles from each flow path and let two half–cycles form a complete cycle if the amplitude at the starting point of one of them has the same value as the amplitude at the stopping point of the other, and vice versa (2–2a + 3–3a, and 4–4a + 5–5a).

The algorithm used to implement the rain flow method in this study is "Rainflow algorithm 1", presented by Downing and Socie (1982).

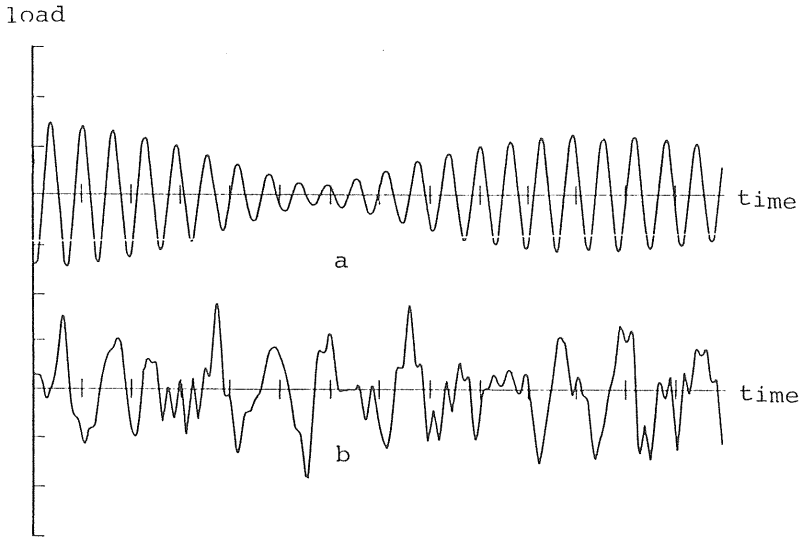

Figure 7.1.2 Samples from random processes. From Wirsching and Light (1980).

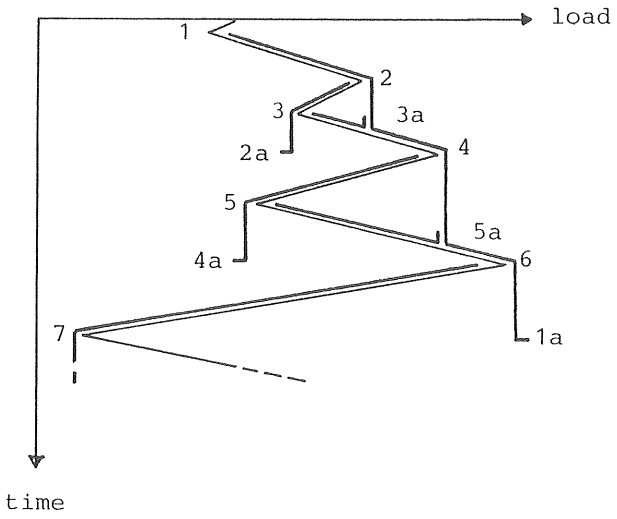

Figure 7.1.3 Rain–flow counting.

7.2 A method of using transfer functions

A method of using transfer functions has been tried for assessing the fatigue. This method is based on the assumption that the transfer function from wave–spectrum to cable load changes moderately with respect to significant wave height, H_s, and spectral peak period, T_p, and that the change with respect to cable mean–load, $\bar{P}$, can be modelled by the variance of the cable load time history, m_{op}. Transfer functions calculated for one set of values of H_s, T_p and $\bar{P}$ can then be applied to situations where the values of H_s, T_p and $\bar{P}$ are different. No attempt has been made to model the change of the transfer function with respect to incoming wave direction, θ, and different sets of random phase angles, ψ_k, of the generating wave (see Section 3.2).

The Fourier transform of the simulated cable load is written

$$C_i = \hat{C}_i e^{j\lambda_i} \qquad (7.2.1)$$

where

$\hat{C}_i$ is the amplitude, and

λ_i is the phase angle of component i

and the transfer function from wave–spectrum, S_i, to the Fourier transform of the cable load is defined

$$V_i = \hat{V}_i e^{j\lambda_i} \qquad (7.2.2)$$

where

$$\hat{V}_i = \hat{C}_i / S_i \quad \text{, when } V_i \text{ is to be applied to sea–states associated with different } H_s \text{ and } T_p. \qquad (7.2.3)$$

Different cable mean–forces, $\bar{P}$, result in quite different values of the cable load variance, and consequently quite different values of the fatigue damage. It is observed that if the amplitude of the transfer function is divided by the standard deviation of the cable load, it can be applied to load cases within a limited interval of cable mean–load around the cable mean–load for which the transfer function was calculated. The amplitude of the transfer function is therefore defined

$\hat{V}_i = \hat{C}_i / (S_i \sqrt{m_{0p}})$, when V_i is to be applied to cable configurations associated with different $\bar{P}$. (7.2.4)

As is mentioned in Chapter 6 the standard deviation of the cable load doesn't vary much from simulation to simulation. Actually, one short simulation of half an hour (real time) is enough to get a correct value.

The transfer function V_i models a transfer from a real parameter, S_i , to a complex parameter, C_i . The phase angles of V_i are set equal to the phase angles of the Fourier transform of the simulated cable load, λ_i . Each simulation, i.e. each choice of random phase angles, ψ_k , of the generating wave will give different values of λ_i .

The basic assumption stated above, is that the transfer function can be regarded as independent of H_s , T_p and $\bar{P}$, i.e.

$$V_i = V_i(\theta, \psi_k) \tag{7.2.5}$$

In Table 7.2.1, fatigue damage, d, calculated with the rain flow algorithm from simulated cable load time histories, is shown. The results vary a great deal from simulation to simulation. Therefore, in the following check of the applicability of the method of using transfer functions (Section 7.3), three different sets of phase angles of the generating wave, ψ_k, are used and the fatigue damage is calculated as average values obtained from these three sets.

Table 7.2.1 Fatigue damage calculated from simulated time series for H_s = 9.3 m, T_p = 14.3 s, $\theta = 270^0$, $\bar{P}$ = 915 kN.

Simulation	Fatigue damage d (10^{-4}/h)
1	0.28
2	0.14
3	0.22
4	0.21
5	0.18
6	0.12
7	0.18
8	0.16
9	0.30

7.3 Applicability of transfer functions

To check the applicability of transfer functions, results from complete simulations were compared with results obtained by transfer functions. The transfer functions were calculated from simulated cable load time histories according to Table 7.3.1.

Table 7.3.1 Calculation of transfer functions.

Transfer function	H_s (m)	T_p (s)	θ (deg.)	$\bar{P}$ (kN)	Set of phase angles
1	9.3	14.3	270	915	a
2	"	"	"	"	b
3	"	"	"	"	c
4	"	17.5	"	"	a
5	"	"	"	"	b
6	"	"	"	"	c

In the figures below the following notation is used; $\bar{d}$ is an average value of the fatigue damage calculated from three complete simulations with the set of phase angles a, b and c, respectively and the values of H_s, T_p, θ, and $\bar{P}$ listed in the figures. (These simulations are also analysed in Chapter 6.) $\bar{d}_1$ is an average value from calculations with transfer functions 1, 2 and 3. $\bar{d}_4$ is an average value from calculations with transfer functions 4, 5 and 6.

Figure 7.3.1 shows that if transfer functions are calculated for H_s = 9.3 m, they can be applied within the interval H_s = 7.8 m to H_s = 12.3 m with good accuracy. Figure 7.3.2 shows that if transfer functions are calculated for T_p = 17.3 s, they can be applied to lower values of T_p, at least down to T_p = 13.8 s. However, no accurate results are obtained when transfer functions are used for larger values of T_p. Figure 7.3.3 shows that if transfer functions are calculated for $\bar{P}$ = 909 kN, they can be applied within the interval 740 kN < $\bar{P}$ < 1000 kN. However, in order to use transfer functions for other values of $\bar{P}$ than the value for which the transfer functions were calculated, the variance of the cable load have to be known.

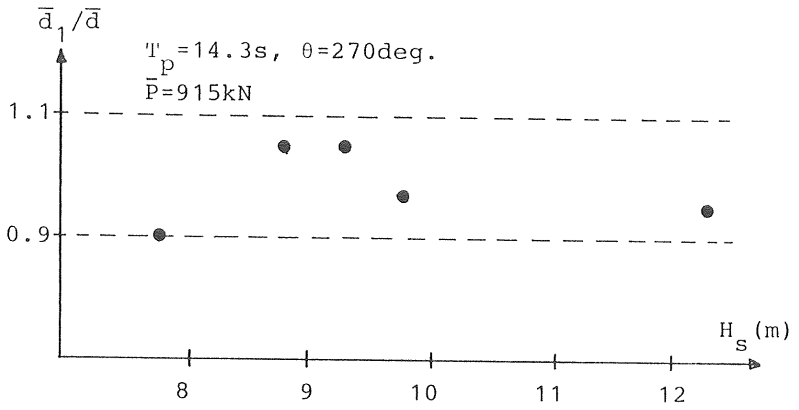

Figure 7.3.1 Ratios between damages calculated with transfer functions and calculated with complete time simulations. The transfer functions were calculated for H_s = 9.3 m.

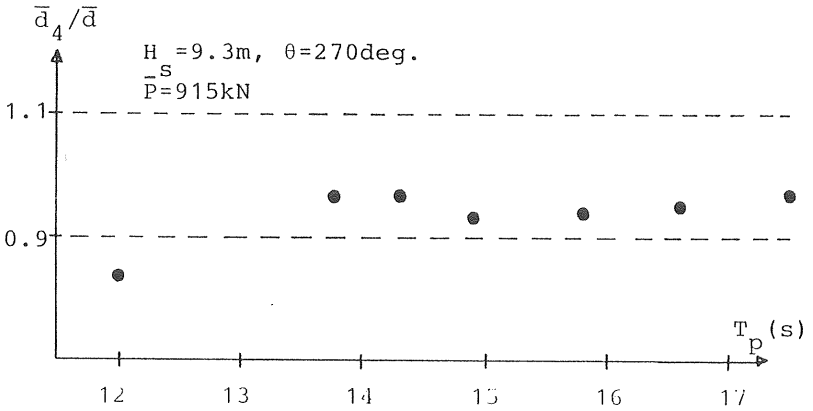

Figure 7.3.2 Ratios between damages calculated with transfer functions and calculated with complete time simulations. The transfer functions were calculated for T_p = 17.5 s.

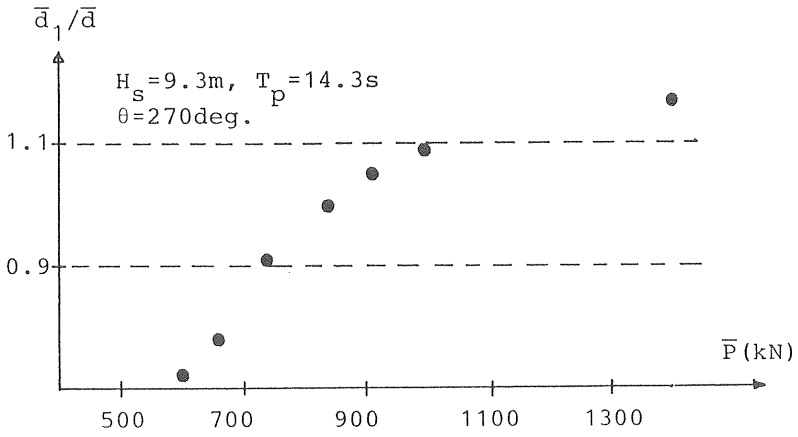

Figure 7.3.3 Ratios between damages calculated with transfer functions and calculated with complete time simulations. The transfer functions were calculated for $\bar{P}$ = 915 kN.

Each transfer function represents only one estimate of fatigue damage. As the estimates vary a great deal from simulation to simulation (see Table 7.2.1), it is necessary to calculate at least four or five transfer functions to get a good average value of the fatigue damage. In addition to this, shorter simulations have to be carried out in order to calculate the variance of the cable load.

7.4 Narrow–band approximation

Simulations of load time history and subsequent load–cycle counting according to the rainflow algorithm are tedious procedures. It would be more practical to use some kind of closed form expression that relates a force (or stress) spectral density function to fatigue damage.

On the assumption that the linear damage rule (see Section 7.1) is applicable and that the S–N curve for the structural member considered has the form $NS^m = K$ (Eq. 2.2.1), it can be shown that the fatigue damage d, in a stationary gaussian narrow band process (i.e. a process which has a spectral density function which is narrow–banded) is

$$d = \frac{n}{K} (2\sqrt{2}\,\sigma)^m \Gamma(\frac{m}{2} + 1) \qquad (7.4.1)$$

where

n	is the total number of cycles,
σ	is the standard deviation of the process and
$\Gamma(x)$	is the gamma function of x.

The distribution of load–cycle ranges counted according to the rain flow algorithm from a time series generated by a stationary Gaussian narrow band process is the Rayleigh distribution:

$$F_S(s) = 1 - \exp(-1/2\ (\frac{s}{2\sigma})^2\ ) \qquad (7.4.2)$$

Wirsching and Light (1980) also suggest the use of Equation 7.4.1 for wide band processes with the number of cycles, n, defined by

$$n = f_0 T \qquad (7.4.3)$$

where

f_0	is the rate of zero up–crossing,
T	is the analysed time.

Introducing (7.4.3) into equation (7.4.1) gives a narrow band approximation of fatigue damage:

$$d_{NB} = \frac{f_0 T}{K} (2\sqrt{2}\,\sigma)^m\ \Gamma(\frac{m}{2} + 1). \qquad (7.4.4)$$

When narrow band approximations are used in this study (section 7.6), the rate of zero up–crossing and the standard deviation are calculated from the spectral moments of the cable load (see Chapter 5):

$$f_0 = \sqrt{m_2/m_0}\ ,$$

$$\sigma = \sqrt{m_0}$$

7.5 Comparing narrow band approximations and simulations

There are two purposes of this comparison. The first is to see how accurate the narrow band approximation is for the cable load processes studied in this report, and the second is to find an S–N curve defined by Equation 2.2.1 which can be used as a representation of the sample S–N curve (Figure 2.2.2) in the narrow band approximation .

Five sets of nine one–hour (real time) simulations are performed. For each simulation the cable mean–load $\bar{P}$ and the number and ranges of load–cycles are calculated directly from the cable load time histories. The standard deviation, σ, the rate of zero up–crossing, f_o, and the spectral width, ε, are calculated from cable load spectra as described in section 7.4. Table 7.1 shows the input to the simulations and average values over each set of simulations of $\bar{P}$, σ, f_o and ε. UBL is the breaking load, which is set to 4290 kN (see Section 2.2).

Table 7.5.1. Simulated one–hour long cable load time histories.

No	Sea–state			$\bar{P}$(kN)	σ(%UBL)	f_0(Hz)	ε
	H_s(m)	T_p(s)	θ(deg)				
1–9	7.8	12.0	285	520	1.3	0.085	0.36
10–18	12.3	16.5	315	630	1.6	0.068	0.47
19–27	12.3	16.5	295	630	2.4	0.067	0.42
28–36	9.3	14.3	270	909	3.7	0.072	0.33
37–45	12.3	16.5	255	630	4.7	0.065	0.38

The fatigue damage is calculated from the simulations either by a method of direct counting of the time series and subsequent averaging over each set or by the use of average values over each set of the spectral parameters (σ and f_o) and the narrow band approximation. Three different S–N curves are used (see Table 7.5.2 and Figure 7.5.1). Curve no. 1 is the sample S–N curve, curves nos. 2 and 3 are S–N curves defined by Equation 2.2.1 and fitted to curve no. 1. Curve no. 4 is used in Section 7.6.

Table 7.5.2 S–N curves

Curve no.	Form	Parameter values
1	Figure 2.2.2	Fatigue limit at S=0.14 UBL
2	$NS^m=K$	m=4.96 $K=509.7\ UBL^m$
3	$NS^m=K$	m=9.08 $K=1.765\ UBL^m$
4	$NS^m=K$	m=3.75 $K=841\ UBL^m$

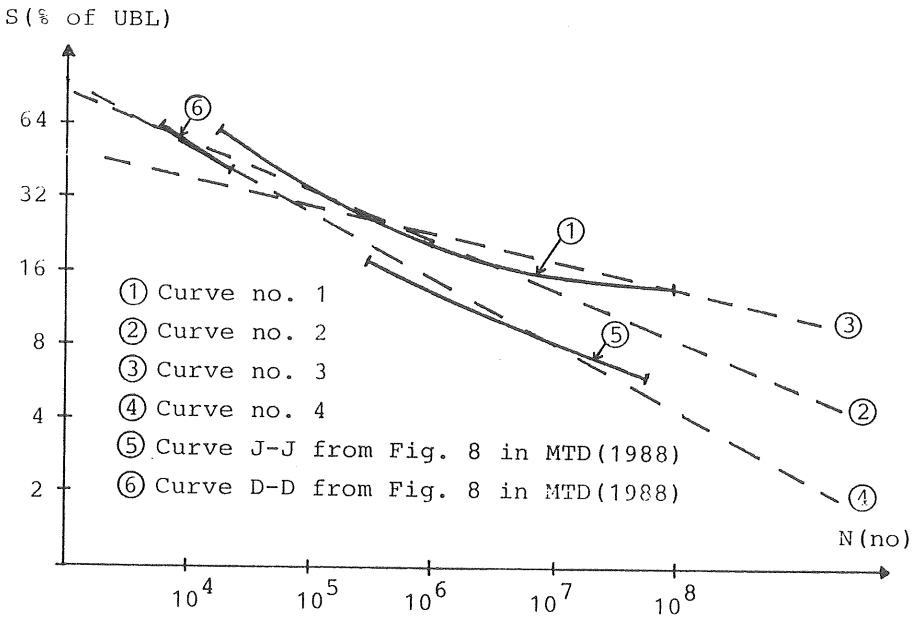

Figure 7.5.1 S–N curves.

The accuracy of the narrow band approximation when applied to the studied cable load processes can be assessed from Table 7.5.3. The values of the fatigue damage obtained with the narrow band approximation are between 8% and 28% lower than the values obtained by direct counting.

Table 7.5.3 Fatigue damage calculated directly and by the narrow band approximation using curve no. 2.

Simulation	Fatigue damage $d(10^{-7}/h)$	
	Calculated directly	Narrow band approximation
1–9	2.04	1.53
10–18	4.47	3.25
19–27	37	28.3
28–36	272	250
37–45	850	740

Table 7.5.4 shows values of the fatigue damage obtained with direct counting and curve no. 1 compared to narrow band approximations calculated using either curve no. 2 or curve no. 3. For cases where the standard deviation σ is within 2.4% – 4.7% of the breaking load (simulation nos. 19–45) curve no. 2 seems to be a good representation of curve no. 1. For cases where σ is less than 1.6 % of the breaking load the fatigue damage is negligible if the fatigue properties of the studied cable follows curve no. 1.

Table 7.5.4 Fatigue damage calculated directly using curve no. 1, narrow band approximated using curve no.2, and narrow band approximated using curve no. 3.

Simulation	Fatigue damage $d(10^{-7}/h)$		
	Calculated directly using curve no.1	Narrow band approximation calculated using curve no. 2	curve no. 3
1–9	0.0	1.53	0.01
10–18	0.08	3.25	0.04
19–27	12.0	28.3	2.5
28–36	249	250	115
37–45	862	740	910

The distribution of load–cycle ranges is analysed for five of the simulations and the distributions are compared with the Rayleigh distribution (Equation 7.4.2) which is the distribution of ranges which would arise from a narrow band process. Table 7.5.5 shows the results. The distributions obtained from the simulations deviate significantly from the Rayleigh distribution. For ranges greater than $S_{.953}$ (see Table 7.5.5, note 2) the simulated distributions show larger values than the Rayleigh distribution. It is this deviation from the Rayleigh distribution that explains the finding that the narrow band approximation is not conservative for the processes studied here.

Table 7.5.5 Cumulative distribution of load–cycle ranges counted by the rain flow algorithm and the Rayleigh distribution (Eq. 7.4.2).

Simulation	Ranges divided by σ						
	$S_{.02}$[2]	$S_{.05}$	$S_{.20}$	$S_{.50}$	$S_{.953}$	$S_{.993}$	S_{max}
1	0.020	0.165	0.934	2.11	5.08	6.07	9.91
10	0.030	0.140	0.721	1.83	5.27	6.86	9.65
27	0.039	0.121	0.831	1.88	5.18	6.49	7.85
28	0.023	0.162	0.924	2.09	4.99	6.75	8.80
45	0.049	0.130	0.740	1.96	5.21	6.41	6.64
Rayleigh dist.	0.400	0.640	1.340	2.35	4.95	6.30	6.82[3]

Notes: 1) Each simulated time history consists of about 300 cycles.
2) The probability that $S<S_x$ is x.
3) $F_s(6.82) = 1-1/300$

7.6 Solving the sample problem by using narrow band approximations

The calculation of the time to fatigue failure is performed for cables nos. 1–4 of the sample platform and sea–states with $H_s>7.5$ m using observations of the wave climate at Haltenbanken from the years 1980–1986 and the narrow band approximation. The sample S–N curve is approximated by curves no 2 (defined in Section 7.5). For comparison a calculation is also carried out with curve no.4, which is an S–N curve representing a wire cable of another type and/or worse quality than a normal six strand wire rope. It is assumed that the fatigue damage can be ignored for cases where the standard deviation of the cable load time history is smaller than 2.4 % of the breaking load.

Curve no. 4 is defined by equation 2.2.1 and fitted to an S–N curve derived from test results obtained by Fleming which is presented in Figure 9 in MTD (1988). It should be observed that the use of curve no. 4 in the calculations is only a way of illustrating how sensitive the results is with respect to the S–N curve.

The relative frequencies of occurrence of the sea–states for which simulations are performed, are derived from two scatter diagrams in OCEANOR (1987). The scatter diagrams cover the observation period 1980–1986 for a position at Haltenbanken off the Norwegian coast (65°05' N07°34' E). The first scatter diagram shows the number of observations in terms of significant wave height and spectral peak period. The second scatter diagram shows the number of observations in terms of significant wave height and wave direction. The observations were carried out for 17 minutes out of every 3 hours and cover about 70% of the observation period. The scatter diagrams are found in Appendix 4. The relative frequencies of the simulated sea–states are interpreted from the scatter diagrams, as shown in Table 7.6.1.

Table 7.6.1. Relative frequencies of sea–states

Sea-state			Data from OCEANOR (1987)				Relative frequency
H_s(m)	T_p(s)	θ_c(deg)	T_p(s)	g_1 (10^{-2})	θ_c(deg)	g_2	g (10^{-2})
7.8	12.0	360	<13.5	0.33	330– 45	0.06	0.020
		300			270–330	0.14	0.046
		240			195–270	0.80	0.264
	15.0	360	>13.5	0.13	330– 45	0.06	0.008
		300			270–330	0.14	0.018
		240			195–270	0.80	0.104
8.3	12.0	360	<14.0	0.28	330– 45	0.08	0.022
		300			270–330	0.16	0.045
		240			195–270	0.76	0.213
	16.0	360	>14.0	0.13	330– 45	0.08	0.010
		300			270–330	0.16	0.021
		240			195–270	0.76	0.099
8.8	13.0	360	<15.0	0.22	330– 45	0.15	0.033
		300			270–330	0.24	0.053
		240			195–270	0.61	0.134
	17.0	360	>15.0	0.050	330– 45	0.15	0.008
		300			270–330	0.24	0.012
		240			195–270	0.61	0.030
9.3	12.5	360	<14.0	0.10	330– 45	0.27	0.027
		300			270–330	0.15	0.015
		240			195–270	0.58	0.058
	15.5	360	>14.0	0.045	330– 45	0.27	0.012
		300			270–330	0.15	0.007
		240			195–270	0.58	0.026
9.8	14.0	255	<15.5	0.022	[1]		0.022
	17.0	255	>15.5	0.052			0.052
10.3	16.0	255		0.052			0.052
10.8	14.0	255	<16.0	0.030			0.030
	17.5	255	>16.0	0.022			0.022
11.3	16.0	240		0.030			0.030
11.8	16.5	270		0.007			0.007
12.3	16.5	270		0.007			0.007
Σ				1.507			1.507

Notes: g_1 – frequency relative to the total number of observations.

g_2 – frequency relative to the number of observations of the actual H_s

$g = g_1 g_2$

[1]) distribution with respect to direction is only considered for H_s<9.8m

In Table 7.6.2 the fatigue damage as calculated with narrow band approximations is shown for each sea–state, mooring cable and S–N curve. Also shown are expected values of the fatigue damage which are obtained as weighted sums,

$$d_{exp} = \sum_i g_i d_i$$

where

d_{exp} is the expected value of the fatigue damage per hour of exposure ,

g_i is the relative frequency of occurrence of sea–state i, given in Table 5.4.1.

d_i is the fatigue damage after one hour of exposure to sea–state i.

Table 7.6.2. Weighted fatigue damage, $g_i\ d_i$, calculated with narrow band approximations using S–N curve no. 2.

Sea-state			d (10^{-10}/h)			
H_s(m)	T_p(s)	θ_c(deg)	cable no. 1	cable no. 2	cable no. 3	cable no. 4
7.8	12.0	360		14		
		300				
		240				
	15.0	360		11		
		300				
		240			29	
8.3	12.0	360		20		
		300				
		240				
	16.0	360	4	26		
		300			8	
		240			43	119
8.8	13.0	360	11	95		
		300			24	
		240			80	161
	17.0	360	4	30		
		300			9	
		240			26	42
9.3	12.5	360	24	38		
		300			29	
		240			17	110
	15.5	360	13	71		
		300				
		240			42	
9.8	14.0	255			81	125
	17.0	255			490	16
10.3	16.0	255			500	21
10.8	14.0	255			240	360
	17.5	255			400	14
11.3	16.0	240			96	540
11.8	16.5	270			180	77
12.3	16.5	270			300	140
Σ			56	305	2594	1725

Fatigue failure, by definition (see section 7.1), occurs when the accumulated fatigue damage reaches the value of 1. Thus, the expected time to fatigue failure is found by inverting the expected value of fatigue damage. The expected times to fatigue failure are shown in Table 7.6.3.

Table 7.6.3. Expected time to fatigue failure.

Cable no.	Expected time to fatigue failure (years)	
	Curve no. 2	Curve no. 4
1	20 000	3 600
2	3 700	890
3	440	130
4	660	210

8. CONCLUSIONS

It is concluded that, for a specific sea–state, the fatigue damage is highly dependent on the cable mean–force and on the direction of the cable relative to the wave direction. A proper analysis of the time to fatigue failure should therefore include many load–cases with different cables, wind directions, and cable mean–forces.

The sample problem was formulated with quite a few load–cases and the most appropriate method of analysis, of the two methods considered in this study, was the narrow band method. A similar analysis with the method of using transfer functions would have required more computer time. The analysis of the sample problem with the narrow band method resulted in an expected time to fatigue failure of the mooring cables of 440 years.

The narrow band method is derived for gaussian processes. When applied to the non–gaussian cable force processes studied here, the narrow band method sometimes underestimates the fatigue damage. For the load–cases studied in Section 7.5 the fatigue damages are underestimated by 8% to 28%.

It is concluded that transfer functions from first order wave to cable force, calculated for one wave spectrum, can be used for other wave spectra if the cable configuration, the cable mean force, and the wave direction are not changed.

Some kind of model of the viscous damping of heave motion should be included in the calculation of the platform motion if realistic values of the fatigue damage are to be obtained. In this study, the inclusion of a model of the viscous damping of heave motion resulted in values of the fatigue damage that were about one order of magnitude smaller than values calculated without any viscous damping of heave motion.

The calculation of the fatigue damage is sensitive to the choice of S–N curve. When a "worst case" S–N curve was used instead of the sample S–N curve the time to fatigue failure was reduced by 75%. Another important cable property is the effective modulus of elasticity, E. The use of $E = 5 \cdot 10^{10}$ N/m^2, which is a very low value, instead of a more normal value, $E = 7 \cdot 10^{10}$ N/m^2, reduced the fatigue damage by one order of magnitude. Design values of E are usually larger than $9 \cdot 10^{10}$ N/m^2 for the type of wire rope studied here.

LIST OF SYMBOLS

$\underline{\underline{a}}_i$	6 x 6 added mass matrix of wave component no. i (Eq. 3.2.7)
A	characteristic area of platform normal to the heave direction
A_w	characteristic area used to calculate the wind force on the platform
$\underline{\underline{b}}_i$	6 x 6 radiation damping matrix of wave component no. i (Eq. 3.2.7)
c_l	celerity of a longitudinal tension wave in the cable
$\underline{\underline{c}}$	6 x 6 stiffness matrix (Eq. 3.2.7)
C_{D3}	drag coefficient in the heave direction of the platform
C_{DN}	drag coefficient in the normal direction of the cable
C_{DT}	drag coefficient in the tangential direction of the cable
C_{Dw}	drag coefficient for the calculation of wind force on the platform
C_{FR}	friction coefficient at the sea bottom
C_i	Fourier transform of cable load time history
$\hat{C}_i$	amplitude of C_i
C_M	added mass coefficient
C_{MN}	added mass coefficient in the normal direction of the cable
C_{MT}	added mass coefficient in the tangential direction of the cable
d	fatigue damage
d_{exp}	weighted fatigue damage
d_{NB}	narrow band approximated fatigue damage
$\bar{d}$	average value of fatigue damage
$D(f_i)$	wave drift force coefficient of wave component no. i
E	effective modulus of elasticity

f	frequency
f_i	discrete frequency
f_n	discrete frequency
f_0	lowest frequency of truncated wave spectrum or rate of zero up–crossing
f_2	highest frequency of truncated wave spectrum
f_c	Nyquist critical frequency
f_f	filter frequency
f_m	peak frequency of JONSWAP spectrum
F_d	wave drift force
F_{vi3}	viscous damping force in heave of wave component no. i
F_w	wind force on platform
$\underline{F}_{ei}$	6 x 1 vector containing the wave exciting forces of wave component no. i(Eq. 3.2.7)
$\underline{F}_{ji}$	6 x 1 vector containing the viscous damping forces of wave component no. i
$F_S(s)$	cumulative distribution function of load–ranges
g	acceleration of gravity
g	relative frequency of occurrence
g_1	relative frequency of occurrence
g_2	frequency relative to the total number of observations of the actual H_s
$h(t)$	complex signal
h_k	sampled time series, k=0,1,2,...N–1
h'_k	filtered time series, k=0,1,2,...N–1
$H(f)$	Fourier transform of h(t)
H_n	discrete Fourier transform of h_k , n=0,1,2,...N–1
H_s	significant wave height
H'_n	H_n reduced
H'_s	significant wave height of truncated wave spectrum

K	constant used in Equation (2.2.1) or cable stiffness (Eq. 3.3.1)
L	length of the finite elements of the cable
m	constant used in Equation (2.2.1)
m_i	i–th moment of spectrum
m_{ip}	i–th moment of cable load spectrum
m_{iw}	i–th moment of truncated wave spectrum
$\underline{\underline{m}}$	6 x 6 mass matrix (Eq. 3.2.7)
n_{el}	number of finite elements
N	number of load–cycles or number of components
$p(\psi_i)$	probability density function of ψ_i
$P_h(f)$	spectral density
$\bar{P}$	mean value of cable load
S	load range
$S(f)$	spectral density
S_n	discrete spectral density at frequency f_n
S_x	value of the cumulative distribution function of load–ranges at the probability x
t	time
T	time length of simulated wave
T_{2p}	zero up–crossing period of cable load time series
T_{2w}	zero up–crossing period of truncated wave spectrum
T_{ik}	transfer function from the i–th wave component to the platform motion in the k–th degree of freedom
T_p	spectral peak period
$\hat{T}_{ik}$	amplitude of T_{ik}

U_{10}	velocity of the wind 10 m above the water surface
UBL	actual or ultimate breaking load
v_c	current velocity
V_i	transfer function from wave to cable load
$\hat{V}_i$	amplitude of V_i
x_1	horizontal coordinate of cable (Fig. 3.3.1)
x_2	vertical coordinate of cable (Fig. 3.3.1)
$x_k(t)$	complex motion of the platform in the k–th degree of freedom
x_{ki}	platform motion in k–th degree of freedom of wave component no. i
$\underline{x}_i$	6 x 1 vector containing the platform motions of wave component no. i
α	shape parameter of JONSWAP spectrum
γ	shape parameter of JONSWAP spectrum
γ_0	cable mass per unit length
Δf	frequency interval
Δt	time interval
ε_p	spectral width of cable load spectrum
ε_w	spectral width of truncated wave spectrum
ψ_i	phase angle of wave component no. i
ϕ_{ik}	phase angle of T_{ik}
λ_i	phase angle of C_i and V_i
ρ_a	density of air
ρ_w	density of water
σ	shape parameter of JONSWAP spectrum (Eq. 4.2.1) or standard deviation
η_i	amplitude of wave component no. i
θ	direction relative to the heading of the platform (Eq. 3.1.1)
θ_c	compass direction (Eq. 3.1.1)
$\zeta(t)$	wave elevation as a function of time
$\zeta_c(t)$	complex wave elevation as a function of time
$\zeta_{ci}(t)$	complex wave elevation of wave component no. i

LIST OF FIGURES

LIST OF TABLES

REFERENCES

Avedal, C. and Erikson, J. (1983): Stanafas, datorprogram för statisk analys av förankringssystemet hos en semisubmersibel (Stanafas, a computer program for the statical analysis of the mooring system for a semisubmersible), Examensarbete 1983:1, Department of Hydraulics, Chalmers University of Technology, Göteborg.

Bergdahl, L and Rask, J. (1987): Dynamic vs. quasi static design of catenary mooring system. Offshore Technology Conference, Proceedings, Paper No. 5530, Houston, Texas.

Brigham, E. O. (1974): The Fast Fourier Transform. Prentice–Hall, Englewood Cliffs, N.J.

Consafe Group (1982): Operation manual, Safe Holmia.

DnV, Det norske Veritas (1985): Column stabilized units (Semisubmersible platforms), Classification notes No. 31.4, Norway.

Dietrich, G. and Kalle, K. (1965): Allgemeine Meereskunde, Gebrüder Borntraeger, Berlin–Nikolassee.

Downing, S.D. and Socie, D.F. (1982): Simple rainflow counting algorithm, International Journal of Fatigue, January 1982.

Elgar, S., Guza, R.T. and Seymor, R.J. (1985): Wave group statistics from numerical simulation of a random sea. Applied Ocean Research, Vol. 7, No. 2.

Faltinsen, O.M. and Michelsen F.C. (1975): Motions of large structures in waves at zero Froude number, Det norske Veritas, publication no. 90.

Hasselman, K. et al. (1973): Measurements of wind–wave growth and swell decay during the Joint North Sea Wave Project (JONSWAP), Ergänzungsheft zur Deutschen Hydrographischen Zeitschrift, Reihe A (8^0), Nr. 12, Hamburg.

Houmb, O.G. and Øyan, T. (1977): On the statistical properties of 115 wave records from the Norwegian shelf, Division of Port and Ocean Eng., The University of Trondheim, Trondheim, Norway.

Houmb, O.G. and Oyervik, T. (1981): Fits between empirical spectra and the JONSWAP model, Report No. 5, the University of Trondheim, Trondheim, Norway.

Husain, Z. and Cottis, R.A. (1986): The influence of seawater corrosion on the fatigue strength of steel wire rope. International Conference on Fatigue of Engineering Structures and Materials. University of Sheffield, Institution of Mechanical Engineering, Proceedings.

Johansson, P.I. (1976): A finite element model for dynamic analysis of mooring cables. Massachusetts Institute of Technology, Ph.D. Thesis.

Lindahl, J. and Sjöberg, A. (1983): Dynamic analysis of mooring cables, Report Series A:9, Dept. of Hydraulics, Chalmers University of Technology, Göteborg.

Lindahl, J. (1985): Modellförsök med en förankringskabel (Model tests with a mooring cable), Report Series A:12, Dept. of Hydraulics, Chalmers University of Technology, Göteborg.

Lindahl, J. and Bergdahl, L. (1987): MODEX–MODIM users manual, Report Series B:49, Dept. of Hydraulics, Chalmers University of Technology, Göteborg.

MTD, The Marine Technology Directorate Ltd., (1988): Wire ropes in offshore applications, MTD Ltd. publication 88/100, C. R. Chaplin and A. E. Potts (Eds.), London.

NEL, National Engineering Laboratory, (1984): The fatigue of 40 mm diameter six strand wire rope in a sea–water environment. National Engineering Laboratory, Dept. of Industry, Report No. ENER/14 for the UK Dept. of Energy.

OCEANOR, Oceanographic Company of Norway A/S. (1987): Analysis of data from Haltenbanken 1974–1986, Summary report 1986, report No. 02 0772 01/04/87.

Palo, P.A. Meggist, D.J. and Nordell, W.J. (1983): Dynamic cable analysis models, 15th Annual Offshore Technology Conference in Houston, Texas, Proceedings, paper No. OTC 4500.

Press, W. H., Flannery, B.P., Teukolsky, S.A. and Vetterling, W.T. (1986): Numerical Recipes: the art of scientific computing, Cambridge University Press.

Reemsnyder, H. S. (1972): The mechanical behaviour and fatigue resistance of steel wire, strand and rope, Homer Research Laboratories, Bethlehem Steel Corporation, Bethlehem PA.

Safe Offshore, (1986): Technical report 207, Göteborg.

Scanrope A/S (1984): Test of anchor line from "Safe Concordia", report No. 1112, Tönsberg, Norway.

VERITEC (1983): WADIF wave forces on large objects of arbitrary form User's manual NV1459, A/S VERITEC, Høvik, Norway.

Wirsching, P.H. and Light, M.C. (1980): Fatigue under wide band random stresses. Journal of the Structural Division, Proceedings of the American Society of Civil Engineers, Vol. 106, No. ST7.

Zimmerman, Z. and Reemsnyder, H.S. (1985): Axial corrosion of wire rope, 17th Annual Offshore Technology Conference, Proceedings, paper no. OTC 5027, Houston, Texas.

APPENDIX 1

Hydrodynamic coefficients and wave exciting forces

A computer program, WADIF, developed by Det norske Veritas (VERITEC, 1983) is used to compute the hydrodynamic coefficients and the wave exciting forces. The structure/fluid problem is formulated according to first order potential theory and the model uses a sink source technique to solve the Laplace equation. The model is described briefly below, and in detail by Faltinsen and Michelsen (1975).

The fluid is assumed to be ideal and the flow to be irrotational. It is then possible to use the velocity potential ϕ ($\underline{x}$,t) as a description of the flow. The waterdepth is assumed to be finite and constant, and the extension of the free surface is assumed to be infinite in all directions. The motions of the structure and of the free surface of the fluid are assumed to be small, which justifies a linearization of the boundary conditions at the structure and at the free surface.

The structure is assumed to be rigid, and therefore any motion of the structure can be described by motions in six degrees of freedom, i.e. three translations and three rotations. A Cartesian coordinate system Oxyz is defined with its origin in the free mean water surface and its z–axis positive upwards and oriented through the centre of gravity. The vector of motion is denoted by $\underline{x}$ and contains the following elements:

x_1 = translation in the x–direction	= surge motion
x_2 = translation in the y–direction	= sway motion
x_3 = translation in the z–direction	= heave motion
x_4 = rotation about the x–axis	= roll motion
x_5 = rotation about the y–axis	= pitch motion
x_6 = rotation about the z–axis	= yaw motion

For stationary conditions the potential can be written as a sum of the contributions from the incoming wave, the scattered wave and the radiated wave respectively:

$$\phi = \phi_I + \phi_S + \phi_R \qquad \text{(A1.1)}$$

The potentials can be factorized into one space–independent part and one time–independent part. Further, the potential for the radiated wave can be split into contributions from each mode of motion.

$$\phi_I = \phi_o \, e^{-j\omega t} \tag{A1.2}$$

$$\phi_S = \phi_7 \, e^{-j\omega t} \tag{A1.3}$$

$$\phi_R = \sum_{i=1}^{6} \phi_i \dot{x}_i \tag{A1.4}$$

where

$$\phi_o \, e^{-j\omega t} = \left\{ \frac{g\zeta_a}{\omega} \cdot \frac{\cosh k(z+h)}{\cosh kh} \right\} e^{j(kx \cos \beta + ky \sin \beta - \omega t)} \tag{A1.5}$$

ϕ_k is the time–independent potential, k=0,1,2,...7
ζ_a is the wave amplitude
β is the direction of propagation
k is the wave number
ω is the wave frequency
$\dot{x}_i$ is the time derivative of displacement in mode i

It can be shown that ϕ_k, k=0,....,7 must satisfy the Laplace equation,

$$\frac{\partial^2 \phi_k}{\partial x^2} + \frac{\partial^2 \phi_k}{\partial y^2} + \frac{\partial^2 \phi_k}{\partial z^2} = 0, \tag{A1.6}$$

the free surface boundary condition,

$$-\omega^2 \phi_k + g \frac{\partial \phi_k}{\partial z} = 0 \text{ at } z=0, \tag{A1.7}$$

and the boundary condition at the bottom

$$\frac{\partial \phi_k}{\partial z} = 0 \text{ at } z=-h. \tag{A1.8}$$

Further the potential for the scattered wave and the potential for the radiated wave are assumed to fulfill a radiation condition and finally the following boundary conditions must be satisfied at the surface of the structure.

$$\frac{\partial \phi_k}{\partial n} = n_k, \; k=1,..,6 \tag{A1.9}$$

$$\frac{\partial \phi_7}{\partial n} = -\frac{\partial \phi_o}{\partial n} \tag{A1.10}$$

where

$\partial/\partial n$ is the normal derivate in the direction of the outward normal to the surface of the structure

$\underline{n} =$ (n_1, n_2, n_3)

$\underline{r} \times \underline{n} =$ (n_4, n_5, n_6)

$\underline{n}$ is the outward normal to the surface of the structure

$\underline{r}$ is the position vector.

The potentials ϕ_k, k=1,...,7, may be expressed in terms of surface distributions of sources,

$$\phi_k (x,y,z) = \iint_S Q_k (\xi,\eta,\zeta) G(x,y,z;\xi,\eta,\zeta) ds \qquad \text{(A1.11)}$$

where

S is the average wetted surface of the structure,

Q_k is the unknown source density function. (ξ,η,ζ), are the coordinates of a point on S,

G is the Green function (source potential) that satisfies the boundary conditions (A1.7), (A1.8), and the radiation condition.

The source densities are found by satisfying the structure boundary conditions (A1.9) and (A1.10). This results in the following two–dimensional Fredholm integral equations of the second kind over the surface S

$$-2\pi Q_k (x,y,z) + \iint_S Q_k (\xi,\eta,\zeta) \frac{\partial}{\partial n} (G(x,y,z;\xi,\eta,\zeta)) \, ds =$$

$$= \begin{cases} n_k & , \quad k = 1,..,6 \\ -\dfrac{\partial \phi_o}{\partial n} & , \quad k = 7 \end{cases} \qquad \text{(A1.12)}$$

Equation (A1.12) is solved by approximating the structure surface by a large number of plane quadrilateral elements, over each of which the source density is assumed to be constant. This transforms the integral equation into a set of linear algebraic equations in the unknown source densities on the elements. When the source densities Q_k have been computed from this set of equations the normalized potentials ϕ_k, k=1,..,7, may be obtained from Equation (A1.11), using a similar integration procedure. The added mass and damping coefficients are then, by definition,

$$a_{ik} = -\rho \, \mathrm{Re} \left(\iint_S \phi_k n_i ds \right) \qquad \text{(A1.13)}$$

$$b_{ik} = -\rho\omega \mathrm{Im} \left(\iint_S \phi_k n_i ds \right) \qquad \text{(A1.14)}$$

$i = 1,..,6, \;\; k = 1,..,6$

The wave exciting forces are obtained from the potentials ϕ_I and ϕ_S by using the linearized Bernoulli's equation to obtain the dynamic pressure

$$p = \rho\omega \, j(\phi_o + \phi_7) \, e^{-j\omega t}, \qquad \text{(A1.15)}$$

and then integrating this pressure over the surface S,

$$F_{ei} = -\iint_S p n_k ds, \;\; k=1,2,..,6 \qquad \text{(A1.16)}$$

APPENDIX 2

The dynamic cable model MODEX.

The dynamic cable model used in this study was developed by Lindahl (Lindahl and Sjöberg, 1983). The model has been thoroughly tested (see Chapter 1). A short description of the model is given below. See Lindahl and Sjöberg (1983) and Lindahl and Bergdahl (1987) for further information.

The cable is regarded as a long slender structure, i.e. the only internal force considered is the tangential tension T. T is related to the stiffness of the cable by the constitutive relation Eq. A2.1. Hydrodynamic forces acting on the cable are analysed by use of the Morison equation. The basic analysis results in non–linear partial differential equations of motion (equations A2.2). These equations are transformed to a system of ordinary time–dependent differential equations (equations A2.3) using a finite element formulation. Positions, displacements and velocities are assumed to have a linear variation over each finite element while accelerations are piece–wise constant in order to obtain an easiliy invertible mass matrix. The equations A2.3 are solved by means of an explicit integration method. The sea bottom is modelled as stiff and energy absorbing and a frictional force (equation A2.4) is added at the nodes which are at the sea bottom.

The cable is modelled in a cartesian coordinate system using a reference configuration (R) and an actual configuration (A). The position vector of the reference configuration $\underline{x}_0$ is a function of the unstretched length s_0 of the cable; $\underline{x}_0=\underline{x}_0(s_0)$. The actual configuration is a function of time t and its position vector $\underline{x}$ is defined $\underline{x}=\underline{x}(s_0,t)$. The displacement from R to A is denoted by the vector $\underline{u}$, $\underline{u}=\underline{u}(s_0,t)$, $\underline{u}=\underline{x}-\underline{x}_0$. The stretched lenght in the actual configuration is denoted by s.

The constitutive relation between tangential tension and stiffness is

$$T=K\tilde{\varepsilon}(1+\varepsilon) + c\dot{\varepsilon} \qquad \text{(A2.1)}$$

where

T	is the tangential tension,
K	is the stiffness,
$\tilde{\varepsilon}$ and ε	express the elongation;
$\dot{\varepsilon}$	is the rate of strain
c	is the coefficient of internal damping

$$\tilde{\varepsilon} = \tfrac{1}{2}\left(\left(\frac{\partial s}{\partial s_0}\right)^2 - 1\right),$$

$$\varepsilon = \frac{\partial s}{\partial s_0} - 1.$$

The basic equations of motion are

$$\gamma_0\,\underline{\ddot{u}} + C_4(1+\varepsilon)\underline{\ddot{u}} - \frac{C_4}{1+\varepsilon}(\underline{\ddot{u}}\cdot\underline{x}')\underline{x}' - \frac{\partial}{\partial s_0}\left((K\tilde{\varepsilon} + c\,\frac{\dot{\tilde{\varepsilon}}}{1+2\tilde{\varepsilon}})\underline{x}'\right) - \underline{f} = 0 \quad \text{(A2.2)}$$

where

γ_0 is the cable mass per unit of unstretched length,

$\underline{\ddot{u}}$ implies $\dfrac{\partial^2}{\partial t^2}(\underline{u})$,

$\underline{x}'$ implies $\dfrac{\partial}{\partial s_0}(\underline{x})$,

$\underline{f}$ is a vector containing the gravity forces, the hydrostatic forces and the drag forces acting on the cable, $\underline{f} = \underline{f}(s_o,t)$,

$$C_4 = C_{MN}\frac{\pi d_o^2}{4}\zeta_v,$$

where

C_{MN} is the hydrodynamic mass coefficient

d_o is the diameter of the unstretched cable

ζ_v is the water mass density.

The equations of motion of the discretized system are

$$\underline{\underline{M}}\,\underline{\ddot{p}} = \underline{R} - \underline{F} \qquad \text{(A2.3)}$$

where

$\underline{\underline{M}}$ is the mass matrix, $\underline{\underline{M}}$ is a function of displacements,

$\underline{p}$ is a vector which contains the nodal displacements,

$\underline{R}$ is a vector derived from the gravity forces, the hydrostatic forces and the drag forces, $\underline{R}$ is a function of both displacements and velocities.

$\underline{F}$ is a vector that represents the internal force of the cable, $\underline{F}$ is a function of displacements.

The frictional force $\underline{F}_f$ which is added to a node, k, that lies on the sea bottom has the opposite direction to the displacement velocity of the node and the absolute value

$$|\underline{F}_f| = \begin{cases} \frac{\dot{p}_a}{c_v}\ \mu\ |\underline{R}^{(1)}_{(k)}|, & \dot{p}_a \le c_v \\ \mu |\underline{R}^{(1)}_{(k)}|, & \dot{p}_a \ge c_v \end{cases} \qquad \text{(A2.4)}$$

where

$\dot{p}_a$ is the velocity of node k,

c_v is a constant,

μ is the coefficient of friciton beteween the cable and the bottom,

$\underline{R}^{(1)}_{(k)}$ is the resultant of gravity forces and lift forces at node k.

The upper limit of the time step for the explicit integration method is

$$\Delta t < l_{j\,min}/c_l, \qquad \text{(A2.5)}$$

where

l_{jmin} is the length of the shortest finite element,

c_l is the celerity of the longitudinal tension,

$c_l = \sqrt{K/\gamma_o}$.

APPENDIX 3

Geometrical transformations

Coordinate systems

The Cartesian coordinate systems are called the global (or G), equilibrium (or E), body (or B), and anchor system (or A) respectively.They are used to transform the motion of the platform to the motion of the upper end (fairlead) of the mooring cable.

The global system is an earth–fixed system with its origin in the free mean water surface and oriented through either the operational position, i.e. adjacent to the fixed installation, or the stand–off position, i.e. about one hundred meter away from the fixed installation. The z–axis is positive upwards (see Figure 1).

The equilibrium system is an earth–fixed system defined by the equilibrium position of the platform. The equilibrium system has its origin in the free mean water surface and is oriented through the center of the platform. The x–axis is positive in the forward direction of the platform.

The body system coincides with the equilibrium system when the platform is at rest and then follows the platform in its motion.

The anchor system is earth fixed with its origin at the anchor of the studied mooring cable. It is oriented in such a way that ,when the platform is in its equilibrium position, the fairlead is in the xz–plane of the system (see Figure 2).

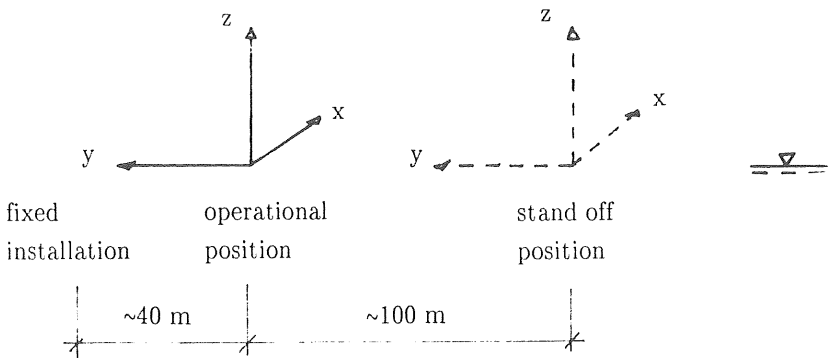

Figure A3.1 The global coordinate system.

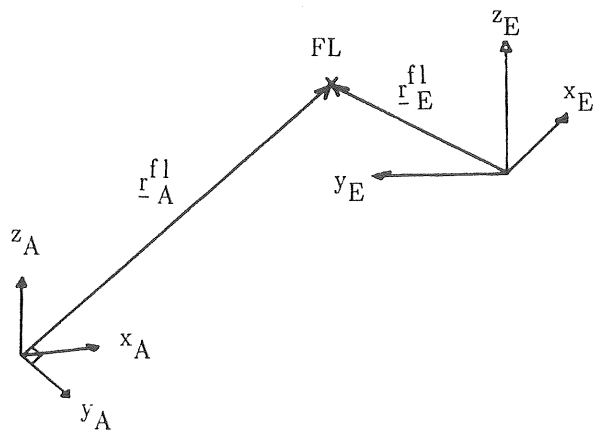

Figure A3.2 The anchor system relative to the equilibrium system.

Coordinate transformation

The aim of the coordinate transformations is to express the motion of the upper end of the cable (i.e. the fairlead) in the coordinate system that is used in the dynamic cable model. This chapter describes a procedure for coordinate transformations and then the procedure is applied to the actual problem.

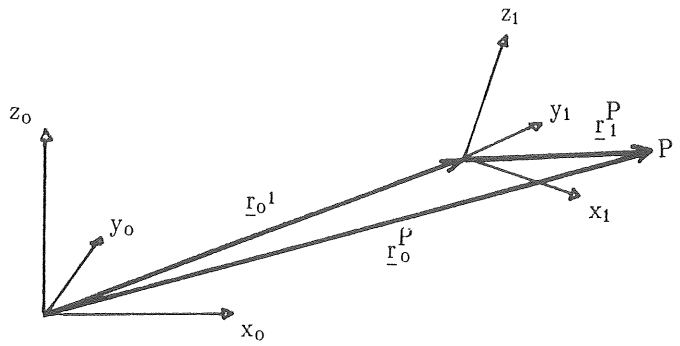

Figure A3.3 Relation between two reciprocally translated coordinate system.

Consider two Cartersian coordinate systems, 0 and 1, that are originally coincident (see Figure 3). System 1 is rotated successively around the x, y, and z–axis of system 0 with the angles α, β, and γ respectively. Thereafter, system 1 is translated relative to system 0 so that the origin of system 1 will have the position vector $\underline{r}_o^1$ in system 0. The position vectors $\underline{r}_o^P$, in system 0, and $\underline{r}_1^P$, in system 1, for a point P will then be related in the following way.

$$\underline{r}_o^P = \underline{r}_o^1 + \underline{\underline{R}}_{o1}\, \underline{r}_1^P \qquad \text{(i)}$$

$$\underline{r}_1^P = \underline{\underline{R}}_{o1}^{-1} (\underline{r}_o^P - \underline{r}_o^1) \qquad \text{(ii)}$$

where

$$\underline{\underline{R}}_{o1} = \underline{\underline{R}}_z\, \underline{\underline{R}}_y\, \underline{\underline{R}}_x \qquad \text{(iii)}$$

and

$$\underline{\underline{R}}_x = \begin{bmatrix} 1 & 0 & 0 \\ 0 & \cos\alpha & -\sin\alpha \\ 0 & \sin\alpha & \cos\alpha \end{bmatrix}$$

$$\underline{\underline{R}}_y = \begin{bmatrix} \cos\beta & 0 & \sin\beta \\ 0 & 1 & 0 \\ -\sin\beta & 0 & \cos\beta \end{bmatrix}$$

$$\underline{\underline{R}}_z = \begin{bmatrix} \cos\gamma & -\sin\gamma & 0 \\ \sin\gamma & \cos\gamma & 0 \\ 0 & 0 & 1 \end{bmatrix} \qquad \text{(iv)}$$

The actual problem is to find the position vector $\underline{r}_A^{fl}$ for the fairlead, fl, in the anchor system, A. From the static calculations with STANAFAS (Avedal and Ericson, 1983) and the chosen mooring pattern the following are known.

$\underline{r}_G^E$ the position vector in the global system, G, for the origin of the equilibrium system, E;

$\underline{r}_G^A$ the position vector in the global system for the origin of the anchor system;

$\underline{r}_E^B$ the position vector in the equilibrium system for the origin of the body system. $\underline{r}_E^B$ is a function of time

$\underline{r}_B^{fl}$ the position vector in the body system for the fairlead

$\alpha_{GB},\beta_{GB},\gamma_{GB}$ the rotation of the equilibrium system around the x–, y–, and z–axes, respectively, of the global system ($\alpha_{GB}=\beta_{GB}=0$).

$\alpha_{EB},\beta_{EB},\gamma_{EB}$ the rotation of the body system around the x–, y–, and z–axis, respectively, of the equilibrium system. α_{EB}, β_{EB}, and γ_{EB} are functions of time.

First, the position vector in the equilibrium system for the fairlead, $\underline{r}_E^{fl}$, is calculated using Eq. (i),

$$\underline{r}_E^{fl} = \underline{r}_E^B + \underline{\underline{R}}_{EB}\, \underline{r}_B^{fl} \qquad (v)$$

where

$$\underline{\underline{R}}_{EB} = \underline{\underline{R}}_z (\gamma=\gamma_{EB})\, \underline{\underline{R}}_y (\beta=\beta_{EB})\, \underline{\underline{R}}_x (\alpha=\alpha_{EB})$$

and

R_x, R_y, R_z are defined in Eq. (iv)

As it is known that $\alpha_{GE}=\beta_{GE}=0$ the *matrix* for transformation from the global system to the equilibrium system is readily found;

$$\underline{\underline{R}}_{GE} = \underline{\underline{R}}_z (\gamma=\gamma_{GE})$$

Now it is possible to relate the anchor system to the equilibrium system. The position vector in the equilibrium system of the origin of the anchor system, $\underline{r}_E^A$, is found by using Eq. (ii)

$$\underline{r}_E^A = \underline{\underline{R}}_{GE}^{-1} (\underline{r}_G^A - \underline{r}_G^E) \qquad (vi)$$

To establish the matrix for transformation from the equilibrium system to the anchor system, $\underline{\underline{R}}_{EA}$, the rotation of the anchor system around the equilibrium system has to be defined. This is done by using the first value (t=0) of the time history of the fairlead position:

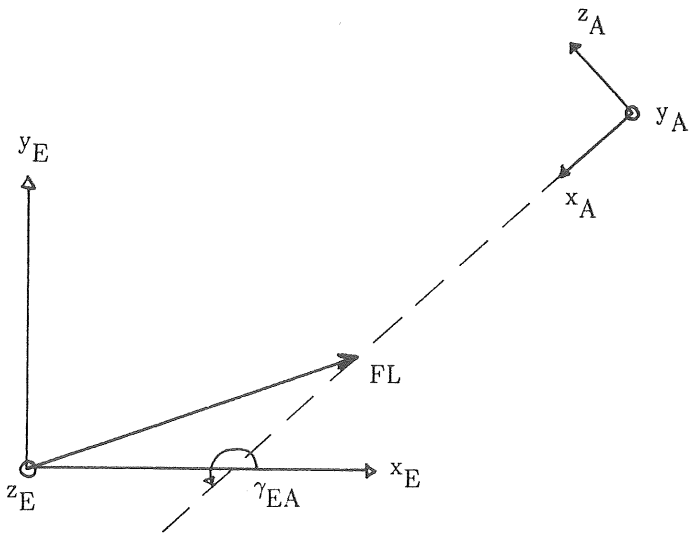

Figure A3.4 Determination of the rotation of the anchor system.

$$\gamma_{EA} = \arctan \frac{y_E^{fl} - y_E^A}{x_E^{fl} - x_E^A} \qquad \text{(vii)}$$

where

x_E^{fl} and y_E^{fl} are the first and second element, respectively, of $\underline{r}_E^{fl}(t=0)$

x_E^A and y_E^A are the first and second element, respectively, of $\underline{r}_E^A$.

Then

$$\underline{\underline{R}}_{EA} = R_z(\gamma = \gamma_{EA})\, \underline{\underline{R}}_x(\alpha = \frac{\pi}{2})$$

and the position vector $\underline{r}_A^{fl}$ in the anchor system for the fairlead can be calculated using Eq. (ii)

$$\underline{r}_A^{fl} = \underline{\underline{R}}_{EA}^{-1}(\underline{r}_E^{fl} - \underline{r}_E^A) \qquad \text{(viii)}$$

APPENDIX 4

Sea state scatter diagrams

The two scatter diagrams below are used in the present study as is described in Section 7.6. They are taken form OCEANOR (1987). The first diagram, Figure A.00.01, shows the number of observations in terms of significant wave height, which in OCEANOR (1987) is called HMO, and spectral peak period, TP. The second diagram, Figure A.00.21, shows the number of observations in terms of significant wave height, HMO, and the wave direction for the waves at the spectral peak, THTP. The wave direction definition is as for winds, i.e. THTP=270° means that the wave travels towards the east.

Figure: A.00.01 <HY/ODAP/86>

```
F R E Q U E N C Y    T A B L E          WAVSTA-C/86.04.02.0 NHL
   .--.   .- O D A P   Oceanographic data acquisition project
 .-    `-.-           Summary report 1986
                      Oceanographic center / Sintef group
 ------------------------------------------------------------
 Location   : H A L T E N  (OUTER)    65°05'N   07°34'E   250M
 Instrument : ODAS 490 491 492 493 494 AND 499 (SEE TAB.: 3.1)
 Sensor     : HIPPY 40A 120A AND 120B          (SEE TAB.: 3.1)
 Sampling   : 3 HOURS / 17 MIN 4 SEC / 0.5 OR 1.0 SEC
 ------------------------------------------------------------
OBSERVATION PERIOD:   80.03.01 AT 00 -- 87.01.01 AT 00
COND: SIGS1<=0.05          HMAX/HMO<=2.6          TU<=26.0
      HMO>0
DATA COVERAGE: .723  HENCE  .929 SATISFIES CONDITION

ABSOLUTE   : TP
DISTR.     : <   :  4.0:  5.0:  6.0:  7.0:  8.0:  9.0: 10.0: 11.0: 12.0: 13.0: 14.0: 15.0: 16.0: 17.0: 18.0: 19.0: 20.0: 21.0:      :MAR.  :CUM. :AVER :STD. :
.............: 4.0:  5.0:  6.0:  7.0:  8.0:  9.0: 10.0: 11.0: 12.0: 13.0: 14.0: 15.0: 16.0: 17.0: 18.0: 19.0: 20.0: 21.0: <   : SUM  :DIS.  :DIS. :AGE  :     :
HMO          ------------------------------------------------------------------------------------------------------------------------------------------------
     <  .50:                    3     1     1     1     2     3     1                                                                :    12 .001  .0009  8.6  2.1:
  .50 - 1.00:   34    64   113   194   183   147    97    63    39    11    11     3     2     2           1     1                  :   965 .072  .0728  7.6  2.2:
 1.00 - 1.50:    8   140   239   334   458   351   238   180   106    59    37    16    12     4     4     2                 1:  2189 .163  .2360  8.1  2.3:
 1.50 - 2.00:        22   206   324   366   462   329   214   108    92    58    28    13    16     5     2     1     1     3:  2250 .168  .4038  8.7  2.4:
 2.00 - 2.50:         1    79   237   325   366   332   240   136   102    63    64    31     8     2     1     1     1     2:  1991 .148  .5522  9.3  2.4:
 2.50 - 3.00:              12   122   203   261   219   183   163   115    73    53    18    11     2     2     2     2     :  1441 .107  .6597  9.9  2.4:
 3.00 - 3.50:                   37   137   196   187   171   138    96    58    40    34    25    12     1     1           1:  1134 .085  .7442 10.5  2.5:
 3.50 - 4.00:                   13    75   130   122   156   122   106    77    36    28    16     9     4                 :   894 .067  .8109 10.9  2.4:
 4.00 - 4.50:                    6    23    88   116   126   126   101    59    49    21    13     6     3                 1:   738 .055  .8659 11.3  2.2:
 4.50 - 5.00:                         9    40    79    86    92    60    55    26    21    19    14     3           2     :   506 .038  .9036 11.8  2.4:
 5.00 - 5.50:                         1    20    44    80    79    62    37    19    18    15     8     8     2     :   393 .029  .9329 12.1  2.3:
 5.50 - 6.00:                               5    18    41    59    48    36    22    16    11     4     4     1     1 :   266 .020  .9527 12.5  2.1:
 6.00 - 6.50:                               4    10    27    49    38    37    13    11     3     3     1     1     :   197 .015  .9674 12.4  1.8:
 6.50 - 7.00:                                     1    11    27    33    26    15     8     6     2                 :   129 .010  .9770 12.9  1.6:
 7.00 - 7.50:                                           5    21    31    16    18     8     2     2     2           :   105 .008  .9849 13.2  1.7:
 7.50 - 8.00:                                           1    11    29     7     7     3     3                 1     :    62 .005  .9895 13.0  1.6:
 8.00 - 8.50:                                           1     8    17    12     8     7     1     1           :    55 .004  .9936 13.4  1.4:
 8.50 - 9.00:                                                 4     9     8     8     2     2           2     1 :    36 .003  .9963 13.9  2.0:
 9.00 - 9.50:                                                 1     2    10     3     2     1                 :    19 .001  .9977 13.8  1.0:
 9.50 -10.00:                                                       1     1     1     3     1     2     1     :    10 .001  .9984 15.6  1.6:
10.00 -10.50:                                                                  2     4           1           :     7 .001  .9990 15.5  1.0:
10.50 -11.00:                                                       1           1     3     1     1           1 :     7 .001  .9995 16.0  1.8:
11.00 -11.50:                                                                  1     2           1           :     4 .000  .9998 15.7  1.1:
11.50 -12.00:                                                                                    1           :     1 .000  .9999 16.0   .0:
12.00 <      :                                                                                   1           :     1 .000  .9999 16.0   .0:
             ------------------------------------------------------------------------------------------------------------------------------------------------
    SUM      :   42   227   652  1268  1781  2071  1794  1588  1290  1013   681   432   267   162    79    37    11     9     8: 13412
MARG.DIS.    :.003  .017  .049  .095  .133  .154  .134  .118  .096  .076  .051  .032  .020  .012  .006  .003  .001  .001  .001 :
CUM. DIS.    :.0031 .0201 .0687 .1632 .2960 .4504 .5841 .7025 .7987 .8742 .9250 .9572 .9771 .9892 .9951 .9978 .9987 .9993 .9999:
AVERAGE      :  .86  1.17  1.46  1.73  1.97  2.29  2.58  2.97  3.54  3.92  4.01  4.07  4.39  4.26  4.55  4.65  4.23  4.69  2.29:
STD          :  .20   .29   .47   .70   .86  1.04  1.20  1.42  1.70  1.91  1.94  2.01  2.25  2.01  2.12  2.07  2.60  2.33   .86:

        HMO          MEAN:  2.73 STD:  1.61
        TP           MEAN:  9.7  STD:  2.8
```

FIGURE: A.00.21<HY/ODAP/86>

F R E Q U E N C Y T A B L E F O R H M 0 A N D T H T P

LOCATION : HALTENBANKEN SAMPLING : 3 HOURS
INSTRUMENT : NORWAVE ODAS SENSOR : DATAWELL HIPPY

RECORDING PERIOD : 1980 - 1986

THTP / HM0	345. 15.	15. 45.	45. 75.	75. 105.	105. 135.	135. 165.	165. 195.	195. 225.	225. 255.	255. 285.	285. 315.	315. 345.	SUM	MARG. PROB.	CUM. PROB.	AVER AGE
< 0.5	1:	:	:	:	:	:	:	:	7:	:	3:	2	13	0.11	0.00115	275.0
0.5 - 1.0	145:	90:	8:	8:	3:	4:	5:	54:	232:	124:	113:	134	920	8.11	0.08226	297.3
1.0 - 1.5	371:	182:	70:	46:	24:	9:	13:	102:	444:	272:	171:	275	1979	17.45	0.25674	306.3
1.5 - 2.0	347:	197:	55:	43:	27:	10:	8:	143:	413:	302:	210:	242	1997	17.61	0.43282	302.1
2.0 - 2.5	339:	151:	55:	30:	33:	10:	23:	187:	381:	209:	144:	182	1744	15.38	0.58658	297.4
2.5 - 3.0	141:	81:	21:	50:	26:	9:	19:	167:	326:	168:	77:	107	1192	10.51	0.69168	271.5
3.0 - 3.5	93:	44:	3:	36:	26:	10:	23:	122:	299:	147:	77:	86	966	8.52	0.77685	263.5
3.5 - 4.0	53:	32:	7:	15:	23:	10:	12:	88:	258:	107:	44:	44	693	6.11	0.83795	257.0
4.0 - 4.5	65:	14:	4:	7:	17:	10:	3:	88:	211:	81:	36:	34	570	5.03	0.88820	257.6
4.5 - 5.0	37:	8:	2:	6:	8:	4:	3:	70:	122:	61:	24:	33	378	3.33	0.92153	259.0
5.0 - 5.5	21:	8:	:	1:	4:	4:	2:	50:	103:	42:	17:	23	275	2.42	0.94578	255.7
5.5 - 6.0	17:	3:	:	:	2:	:	:	39:	83:	21:	6:	18	189	1.67	0.96244	253.1
6.0 - 6.5	15:	3:	:	:	1:	:	:	30:	47:	17:	3:	10	126	1.11	0.97355	255.7
6.5 - 7.0	5:	3:	:	:	:	:	:	21:	35:	16:	1:	11	92	0.81	0.98166	253.9
7.0 - 7.5	2:	:	:	:	:	:	:	13:	31:	11:	4:	5	66	0.58	0.98748	249.5
7.5 - 8.0	2:	:	:	:	:	:	:	17:	19:	6:	3:	2	49	0.43	0.99180	240.6
8.0 - 8.5	1:	1:	:	:	:	:	:	4:	16:	9:	:	1	32	0.28	0.99462	249.0
8.5 - 9.0	1:	1:	:	:	:	:	:	3:	11:	5:	2:	4	27	0.24	0.99700	264.5
9.0 - 9.5	:	3:	:	:	:	:	:	3:	4:	1:	1:	1	13	0.11	0.99815	266.6
9.5 - 10.0	:	:	:	:	:	:	:	:	4:	3:	:		7	0.06	0.99877	253.4
10.0 - 10.5	:	:	:	:	:	:	:	:	2:	2:	:		4	0.04	0.99912	255.8
10.5 - 11.0	:	:	:	:	:	:	:	:	2:	4:	:		6	0.05	0.99965	261.9
11.0 - 11.5	:	:	:	:	:	:	:	:	2:	:	:		2	0.02	0.99982	241.5
11.5 - 12.0	:	:	:	:	:	:	:	:	:	:	:		0	0.00	0.99982	0.0
12.0 - 12.5	:	:	:	:	:	:	:	:	:	1:	:		1	0.01	0.99991	271.0
12.5 - 13.0	:	:	:	:	:	:	:	:	:	:	:		0	0.00	0.99991	0.0
13.0 - 13.5	:	:	:	:	:	:	:	:	:	:	:		0	0.00	0.99991	0.0
13.5 - 14.0	:	:	:	:	:	:	:	:	:	:	:		0	0.00	0.99991	0.0
14.0 - 14.5	:	:	:	:	:	:	:	:	:	:	:		0	0.00	0.99991	0.0
>14.5	:	:	:	:	:	:	:	:	:	:	:		0	0.00	0.99991	0.0
SUM	1656	821	225	242	194	80	111	1201	3052	1609	936	1214	11341			
MARG.PROB.	14.6	7.2	2.0	2.1	1.7	0.7	1.0	10.6	26.9	14.2	8.3	10.7				
CUM.PROB.	.146	.218	.238	.260	.277	.284	.294	.399	.668	.810	.893	1.00				
AVERAGE	2.2	2.1	1.9	2.4	2.8	2.9	2.7	3.2	2.9	2.7	2.2	2.3				
ST.DEV.	1.21	1.13	0.76	0.95	1.16	1.23	1.00	1.67	1.71	1.65	1.30	1.41				

MEAN HM0 : 2.60 MEAN THTP : 283.
ST.DEV.HM0 : 1.53

CHALMERS TEKNISKA HÖGSKOLA
Institutionen för vattenbyggnad

Report Series A

A:1 Bergdahl, L.: Physics of ice and snow as affects thermal pressure. 1977.

A:2 Bergdahl, L.: Thermal ice pressure in lake ice covers. 1978.

A:3 Häggström, S.: Surface Discharge of Cooling Water. Effects of Distortion in Model Investigations. 1978.

A:4 Sellgren, A.: Slurry Transportation of Ores and Industrial Minerals in a Vertical Pipe by Centrifugal Pumps. 1978.

A:5 Arnell, V.: Description and Validation of the CTH–Urban Runoff Model. 1980.

A:6 Sjöberg, A.: Calculation of Unsteady Flows in Regulated Rivers and Storm Sewer Systems. 1976.

A:7 Svensson, T.: Water Exchange and Mixing in Fjords. Mathematical Models and Field Studies in the Byfjord. 1980.

A:8 Arnell, V.: Rainfall Data for the Design of Sewer Pipe Systems. 1982.

A:9 Lindahl, J., Sjöberg, A.: Dynamic Analysis of Mooring Cables. 1983.

A:10 Nilsdal, J–A.: Optimeringsmodellen ILSD. Beräkning av topografins inverkan på ett dagvattensystems kapacitet och anläggningskostnad. 1983.

A:11 Lindahl, J.: Implicit numerisk lösning av rörelseekvationerna för en förankrings-kabel. 1984.

A:12 Lindahl, J.: Modellförsök med en förankringskabel. 1985.

A:13 Lyngfelt, S.: On Urban Runoff Modelling. The Application of Numerical Models Based on the Kinematic Wave Theory. 1985.

A:14 Johansson, M.: Transient Motions of Large Floating Structures. 1986.

A:15 Mårtensson, N., Bergdahl, L.: On the Wave Climate of the Southern Baltic. 1987.

A:16 Moberg, G.: Wave Forces on a Vertical Slender Cylinder. 1988.

A:17 Perrusquía González, G.S.: Part–Full Flow in Pipes with a Sediment Bed. Part one: Bedform dimensions. Part two: Flow resistance. 1988.

A:18 Nilsdal, J–A.: Bedömning av översvämningsrisken i dagvattensystem. Kontrollberäkning med typregn. 1988.

A:19 Johansson, M.: Barrier–Type Breakwaters. Transmission, Reflection and Forces. 1989.

A:20 Rankka, W.: Estimating the Time to Fatigue Failure of Mooring Cables. 1989.

CHALMERS TEKNISKA HÖGSKOLA
Institutionen för vattenbyggnad

Report Series B

B:1 Bergdahl, L.: Beräkning av vågkrafter. (Ersatts med 1979:07) 1977.

B:2 Arnell, V.: Studier av amerikansk dagvattenteknik. 1977.

B:3 Sellgren, A.: Hydraulic Hoisting of Crushed Ores. A feasibility study and pilot–plant investigation on coarse iron ore transportation by centrifugal pumps. 1977.

B:4 Ringesten, B.: Energi ur havsströmmar. 1977.

B:5 Sjöberg, A., Asp, T.: Brukar–anvisning för ROUTE–S. En matematisk modell för beräkning av icke–stationära flöden i floder och kanaler vid strömmande tillstånd. 1977.

B:6 Annual Report 1976/77. 1977.

B:7 Bergdahl, L., Wernersson, L.: Calculated and Expected Thermal Ice Pressures in Five Swedish Lakes. 1977.

B:8 Göransson, C–G., Svensson, T.: Drogue Tracking – Measuring Principles and Data Handling. 1977.

B:9 Göransson, C–G.: Mathematical Model of Sewage Discharge into confined, stratified Basins – Especially Fjords. 1977.

B:10 Arnell, V., Lyngfelt, S.: Beräkning av dagvattenavrinning från urbana områden. 1978.

B:11 Arnell, V.: Analysis of Rainfall Data for Use in Design of Storm Sewer Systems. 1978.

B:12 Sjöberg, A.: On Models to be used in Sweden for Detailed Design and Analysis of Storm Drainage Systems. 1978.

B:13 Lyngfelt, S.: An Analysis of Parameters in a Kinematic Wave Model of Overland Flow in Urban Areas. 1978.

B:14 Sjöberg, A., Lundgren, J., Asp, T., Melin, H.: Manual för ILLUDAS (Version S2). Ett datorprogram för dimensionering och analys av dagvattensystem. 1979.

B:15 Annual Report 1978/79. 1979.

B:16 Nilsdal, J–A., Sjöberg, A.: Dimensionerande regn vid höga vattenstånd i Göta älv. 1979.

B:17 Stöllman, L–E.: Närkes Svartå. Hydrologisk inventering. 1979.

B:18 Svensson, T.: Tracer Measurements of Mixing in the Deep Water of a Small, Stratified Sill Fjord. 1979.

B:19 Svensson, T., Degerman, E., Jansson, B.,Westerlund, S.: Energiutvinning ur sjö– och havssediment. En förstudie. R76:1980. 1979.

B:20 Annual Report 1979. 1980.

B:21 Stöllman, L. E.: Närkes Svartå. Inventering av vattentillgång och vattenanvändning. 1980.

Report Series B

B:22 Häggström, S., Sjöberg, A.: Effects of Distortion in Physical Models of Cooling Water Discharge. 1979.

B:23 Sellgren, A.: A Model for Calculating the Pumping Cost of Industrial Slurries. 1981.

B:24 Lindahl, J.: Rörelseekvationen för en kabel. 1981.

B:25 Bergdahl, L., Olsson, G.: Konstruktioner i havet. Vågkrafter–rörelser. En inventering av datorprogram. 1981.

B:26 Annual Report 1980. 1981.

B:27 Nilsdal, J–A.: Teknisk–ekonomisk dimensionering av avloppsledningar. En litteraturstudie om datormodeller. 1981.

B:28 Sjöberg, A.: The Sewer Network Models DAGVL–A and DAGVL–DIFF. 1981.

B:29 Moberg, G.: Anläggningar för oljeutvinning till havs. Konstruktionstyper, dimensioneringskriterier och positioneringssystem. 1981.

B:30 Sjöberg, A., Bergdahl, L.: Förankringar och förankringskrafter. 1981.

B:31 Häggström, S., Melin, H.: Användning av simuleringsmodellen MITSIM vid vattenresursplanering för Svartån. 1982.

B:32 Bydén, S., Nielsen, B.: Närkes Svartå. Vattenöversikt för Laxå kommun. 1982.

B:33 Sjöberg, A.: On the stability of gradually varied flow in sewers. 1982.

B:34 Bydén, S., Nyberg, E.: Närkes Svartå. Undersökning av grundvattenkvalitet i Laxå kommun. 1982.

B:35 Sjöberg, A., Mårtensson, N.: Regnenveloppmetoden. En analys av metodens tillämplighet för dimensionering av ett 2–års perkolationsmagasin. 1982.

B:36 Svensson, T., Sörman, L–O.: Värmeupptagning med bottenförlagda kylslangar i stillastående vatten. Laboratorieförsök. 1982.

B:37 Mattsson, A.: Koltransporter och kolhantering. Lagring i terminaler och hos storförbrukare. (Delrapport). 1983.

B:38 Strandner, H.: Ett datorprogram för sammankoppling av ILLUDAS och DAGVL–DIFF. 1983.

B:39 Svensson, T., Sörman, L–O.: Värmeupptagning med bottenförlagda slangar i rinnande vatten. Laboratorieförsök. 1983.

B:40 Mattsson, A.: Koltransporter och kolhantering. Lagring i terminaler och hos storförbrukare. Kostnader. Delrapport 2. 1983.

B:41 Häggström, S., Melin, H.: Närkes Svartå. Simuleringsmodellen MITSIM för kvantitativ analys i vattenresursplanering. 1983.

B:42 Hård, S.: Seminarium om miljöeffekter vid naturvärmesystem. Dokumentation sammanställd av S. Hård, VIAK AB. BFR–R60:1984. 1983.

B:43 Lindahl, J.: Manual för MODEX–MODIM. Ett datorprogram för simulering av dynamiska förlopp i förankringskablar. 1983.

Report Series B

B:44 Activity Report. 1984.

B:45 Sjöberg, A.: DAGVL–DIFF. Beräkning av icke–stationära flödesförlopp i helt eller delvis fyllda avloppssystem, tunnlar och kanaler. 1984.

B:46 Bergdahl, L., Melin, H.: WAVE FIELD. Manual till ett program för beräkning av ytvattenvågor. 1985.

B:47 Lyngfelt, S.: Manual för dagvattenmodellen CURE. 1985.

B:48 Perrusquía, G., Lyngfelt, S., Sjöberg, A.: Flödeskapacitet hos avloppsledningar delvis fyllda med sediment. En inledande experimentell och teoretisk studie. 1986.

B:49 Lindahl, J., Bergdahl, L.: MODEX–MODIM. User's Manual. 1987.

B:50 Mårtensson, N.: Dynamic Analysis of a Moored Wave Energy Buoy. 1988.